

# Waveguide-Cavity Scattering in High-Frequency Dissipative Optomechanics

André G. Primo,<sup>1,\*</sup> Pedro V. Pinho,<sup>1,\*</sup> Rodrigo Benevides,<sup>2</sup> Simon Gröblacher,<sup>3</sup> Gustavo S. Wiederhecker,<sup>1</sup> and Thiago P. Mayer Alegre<sup>1,†</sup>

<sup>1</sup>*Gleb Wataghin Institute of Physics, University of Campinas, 13083-859 Campinas, SP, Brazil*

<sup>2</sup>*Department of Physics, ETH Zürich, 8093 Zürich, Switzerland*

<sup>3</sup>*Kavli Institute of Nanoscience, Department of Quantum Nanoscience, Delft University of Technology, Lorentzweg 1, 2628CJ Delft, The Netherlands*

(Dated: January 2, 2023)

The coherent transduction of information between microwave and optical domains is a fundamental building block for future quantum networks. A promising way to bridge these widely different frequencies is using high-frequency nanomechanical resonators interacting with low-loss optical modes. State-of-the-art optomechanical devices require a relatively large photon population in the cavity to enhance the acousto-optic coupling, the heat arising from undesirable optical absorption, however, generates thermal phonons that ultimately hinder their operation in the quantum regime. One way to overcome this problem is by using dissipative optomechanics. In this framework, photons can be scattered directly from a waveguide into a resonator, reducing the need for a large intra-cavity photon population. Hitherto, such dissipative optomechanical interaction was only demonstrated at low mechanical frequencies, precluding the quantum state transfer between photonic and phononic domains. Here, we show the first dissipative optomechanical system operating in the sideband-resolved regime, where the mechanical frequency is larger than the optical linewidth. Exploring this unprecedented regime, we demonstrate the impact of dissipative optomechanical coupling in reshaping both mechanical and optical spectra. Our figures represent a two-order-of-magnitude leap in the mechanical frequency and a tenfold increase in the dissipative optomechanical coupling rate compared to previous works. The present demonstration opens a path to strongly dissipative optomechanical devices with nearly noiseless operation in the quantum regime.

The burgeoning field of cavity optomechanics combines the reliability of long-range information transport using optical photons with the versatility of nanomechanical oscillators. This conjunction enabled a plethora of demonstrations, including high-precision force and displacement sensors [1–3], and the synchronization of mechanical oscillators [4, 5] for signal processing. Furthermore, in high-frequency optomechanical systems, it is possible to actively control the strength of the creation or annihilation scattering process of long-lived phonons [6–9]. This property renders optomechanical systems promising candidates for coherent quantum microwave-to-optical converters [10–15], and quantum memories [16, 17]. However, the thermal phonons generated by absorption of pump photons limit efficient quantum operation [18–21].

In standard dispersive optomechanical devices, the acoustic modes are engineered to shift the optical cavity resonance frequency,  $\omega_0$  [22–24]. As a consequence, only photons confined to the resonator modes are efficiently scattered. This mechanism is quantified by the dispersive optomechanical frequency pulling,  $G_\omega = -\frac{d\omega_0}{dx}$ , where  $x$  is the mechanical displacement amplitude of a given acoustic mode. In most experimental demonstrations to date, the optomechanical coupling rate is rather weak and photons are more likely to be absorbed than interact with the acoustic mode. Consequently, thermal phonons are generated and are responsible for the decoherence of any nonclassical mechanical states.

In dissipatively coupled optomechanical systems, however, the acousto-optic interaction may take place be-

tween the optical excitation channel and the cavity [25–27], e.g., through a mechanical modulation of the bus waveguide-cavity coupling rate  $\kappa_e$ . Its strength is quantified by the dissipative pulling  $G_{\kappa_e} = \frac{d\kappa_e}{dx}$ . In these systems, photons may be scattered directly from the waveguide into the cavity mode, as illustrated in Fig. 1a, reducing the necessity of a large intracavity field. This approach could be used to mitigate the heat due to the absorption of a strong pump field. Nevertheless, these systems are typically hard to engineer, and experimental demonstrations are restricted to the so-called bad-cavity regime [1, 28–30], where the (total) optical dissipation rate is larger than the mechanical frequency ( $\kappa > \Omega$ ), which inhibits their applications to coherent information swap protocols [6]. State-of-the-art devices still need an order-of-magnitude leap in mechanical frequencies to reach this regime, while preserving low optical losses.

Here, we demonstrate an optomechanical system operating in the sideband-resolved regime ( $\Omega/\kappa \approx 10$ ) which displays both dissipative and dispersive optomechanical couplings. Our mechanical modes, operating at  $\Omega/(2\pi) \approx 5.5$  GHz, represent a two-order-of-magnitude increase in frequency when compared to previous dissipative optomechanics devices [1, 29]. We assess the impacts of the mechanically mediated waveguide-cavity interaction by analyzing the acousto-optic transduction in our system, along with optically-induced modifications in the mechanical spectrum, i.e., dynamical backaction [6]. We compare our results with the well-known case of purely dispersive optomechanics and show striking differences,

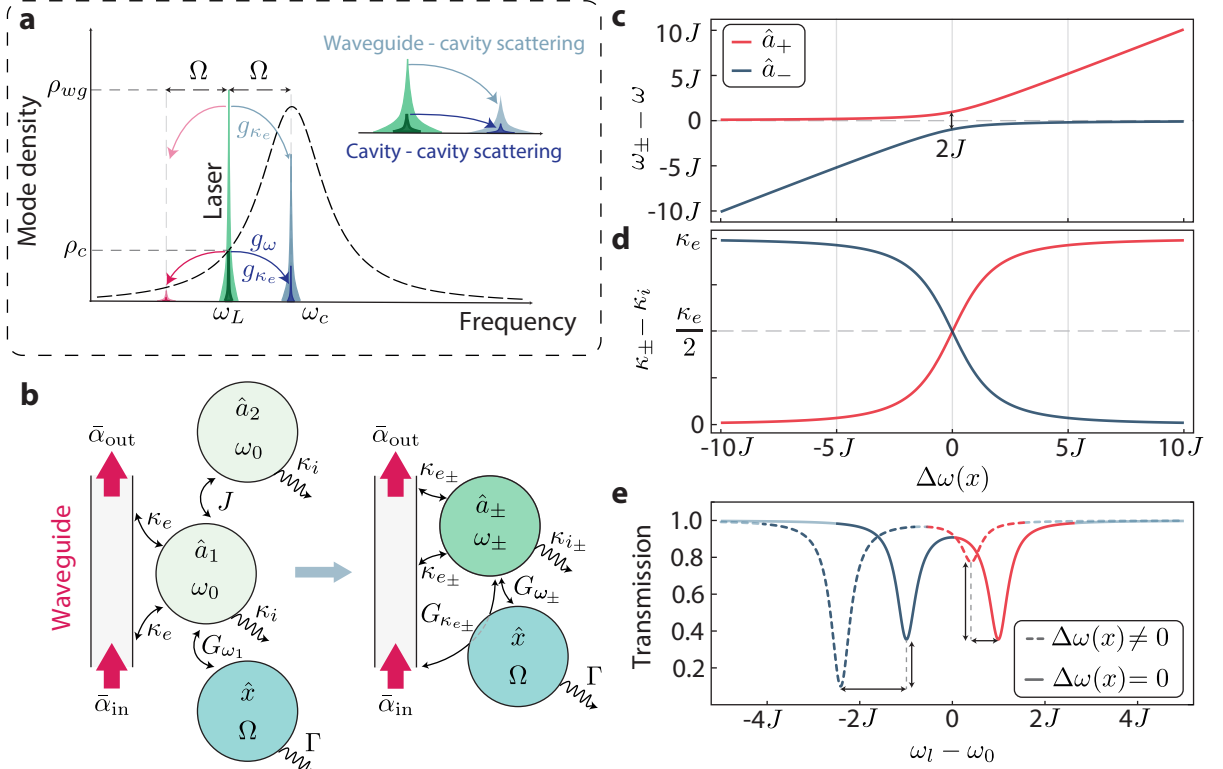


FIG. 1. **a**, Scattering mechanisms in an optomechanical system with both dispersive and dissipative couplings. Photons arriving through a waveguide (mode density  $\rho_{wg}$  - light green) can be inelastically scattered into the cavity field depicted by the light blue/red tones. A similar process occurs for cavity pump photons (mode density  $\rho_c$  - dark green), generating sidebands in dark blue/red. **b**, Diagram for coupled optomechanical cavities with an asymmetric loss induced by the waveguide. The physical response of the system, depicted on the right, necessarily includes a mechanically-dependent extrinsic coupling for both supermodes. **c**, Frequency splitting in strongly-coupled optical cavities and **d**, Supermodes' losses as functions of the frequency detuning between the “bare” resonators,  $\Delta\omega(x)$ . **e**, Transmission spectra for different detuning configurations. The trace colors identify the supermodes as in **c** and **d**. Both the extinction and position are sensitive to mechanically coupled detuning, represented by vertical and horizontal double-headed arrows, respectively.

for instance, the dynamical backaction strength can be either enhanced or suppressed by controlling the interference between dissipative and dispersive contributions. Lastly, we perform coherent spectroscopy [31, 32] of our device and demonstrate, for the first time, optomechanically induced transparency with strong contributions from the dissipative component of the interaction.

In Fig. 1b we show the principle of operation of our device. Two identical optical modes,  $\hat{a}_1$  and  $\hat{a}_2$ , with frequency  $\omega_0$  and intrinsic losses  $\kappa_i$ , are mutually coupled with a photon tunneling rate  $J$ . Photons flow in and out of the system through a waveguide, which carries a coherent field with amplitude  $\bar{\alpha}_{in}$  and drives solely resonator 1 with a rate  $\kappa_e$ . The mode  $\hat{a}_1$  is dispersively coupled to the mechanical mode  $\hat{x}$  with a frequency pulling parameter  $G_{\omega_1}$ . Since  $\hat{a}_1$  and  $\hat{a}_2$  are nearly degenerate, hybridization occurs and the optical supermodes  $\hat{a}_+$  and  $\hat{a}_-$  are formed. In the adiabatic regime, where  $2J \gg \Omega$ , the mechanical mode  $\hat{x}$  is effectively coupled to the supermodes  $\hat{a}_{\pm}$ , instead of the “bare” optical modes  $\hat{a}_1$  and  $\hat{a}_2$  [33–

35]. The “bare” and coupled mode pictures are bridged if we note that  $\hat{x}$  induces a detuning  $\Delta\omega(x) = -G_{\omega_1}\hat{x}$  between  $\hat{a}_1$  and  $\hat{a}_2$ , impacting the supermodes  $\hat{a}_{\pm}$  optical frequencies and losses.

A key aspect of the proposed device relies on the coupled modes' eigenfrequencies. In Fig. 1c and d we show the supermodes' frequencies ( $\omega_{\pm}$ ) and losses ( $\kappa_{\pm}$ ) dependence on  $\Delta\omega(x)$ . When  $|\Delta\omega| \ll J$ , a clear level repulsion arises, and both  $\omega_{\pm}$  are affected by the mechanical motion, corresponding to a dispersive optomechanical coupling  $G_{\omega_{\pm}}$ . Since the resonators 1 and 2 have distinct losses, the loss rates  $\kappa_{\pm}$  are also affected, as shown in Fig. 1d. In our coupled cavity system, the loss asymmetry is caused by additional waveguide extrinsic coupling experienced by cavity 1 ( $\kappa_e$ ) [36]. We note that the supermodes' dissipative coupling  $\frac{d\kappa_{e\pm}}{dx} = \frac{d\kappa_{e\pm}}{d\Delta\omega} \frac{d\Delta\omega}{dx}$  scales with both  $G_{\omega_1} = -\frac{d\Delta\omega}{dx}$  and the slopes,  $\frac{d\kappa_{e\pm}}{d\Delta\omega}$ , of Fig. 1d, becoming stronger the weaker the intercavity coupling  $J$  is. For  $|\Delta\omega| \gg J$ , the supermodes recover the dynamics of two essentially uncoupled oscillators – since their

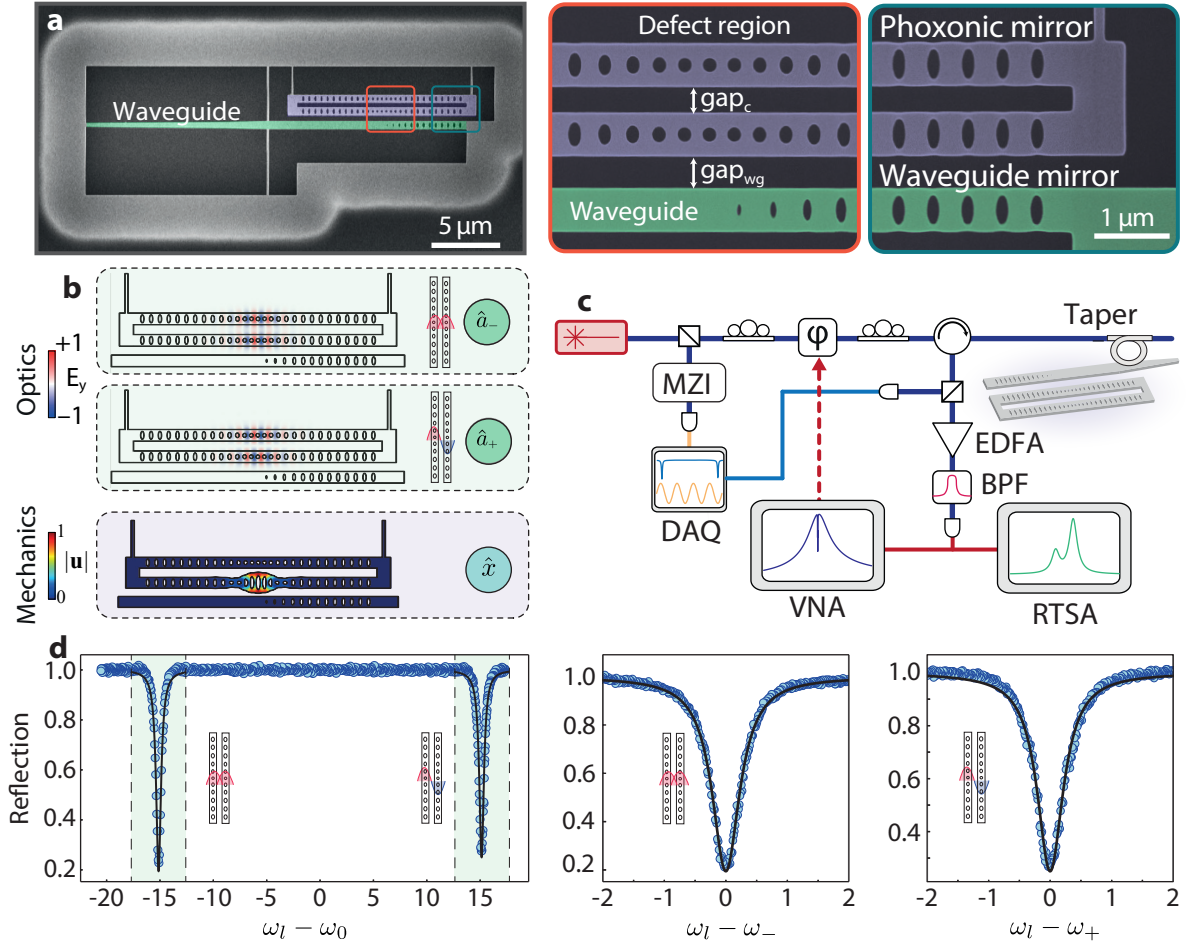


FIG. 2. **a**, Scanning electron micrograph of one of the fabricated devices. The image is false-colored to highlight the coupled optomechanical resonators (blue) and tapered waveguide (green). The defect region is responsible for the high-quality confinement of both mechanical and optical modes. The phoxonic (photonic and phononic) mirror suppresses any mechanical coupling between the two nanobeams. **b**, Finite-element Method simulations of the optical ( $\hat{a}_-$ ,  $\hat{a}_+$ ) and mechanical breathing ( $\hat{x}$ ) modes of our system. Here, we plot the normalized  $y$ -component of the electric field,  $E_y$ , and mechanical displacement  $|\hat{u}|$ . Although both beams support identical mechanical modes, only one is shown for simplicity. **c**, Schematics of the measurement setup. A tunable laser drives our device, which is accessed using a tapered fiber coupled to the integrated waveguide. The thermo-mechanical noise imprinted in the reflected light is collected and characterized with a real-time spectrum analyzer (RTSA). Coherent spectroscopy is performed using a vector network analyzer (VNA), which modulates the phase of the driving field with an electro-optic phase-modulator ( $\phi$ ). Reflection spectra are measured with a DAQ, along with the output of a Mach-Zehnder interferometer (MZI), which provides the relative frequency of our laser. **d**, Normalized reflection spectrum of the cavity, showing symmetric and antisymmetric optical modes. The region around the two resonances is finely-scanned with a laser and fitted to a Lorentzian model, as shown on the right. For the device under analysis,  $\text{gap}_c = 500 \text{ nm}$  and  $\text{gap}_{wg} = 450 \text{ nm}$ .

natural responses are mismatched, no effective hybridization occurs. A detailed mathematical discussion of this interplay is provided in section S1 of the Supplemental Material.

The mechanism leading to the dissipative optomechanical coupling is intuitively understood in terms of the supermode's energy distribution: if  $\Delta\omega = 0$ , the supermodes are roughly symmetric and antisymmetric pairs and photons are evenly split between the “bare” modes  $\hat{a}_1$  and  $\hat{a}_2$ . Deviations from this regime, i.e.,  $\Delta\omega \neq 0$ , lead to an asymmetric optical field distribution among the res-

onators. In such an asymmetric regime, the supermode with larger energy density in cavity 1 (see Fig. 1b) will have larger extrinsic losses, due to its coupling to the bus waveguide. The consequences to the optical spectrum are represented in Fig. 1e, where the mechanically induced optical detuning,  $\Delta\omega(x)$ , lead to variations in both frequencies and extinctions of the  $\hat{a}_\pm$  supermodes.

We implement this scheme using a pair of identically-designed silicon photonic crystal nanobeams, as shown in Fig. 2a (see Methods). An engineered defect in the central region of both nanobeams supports co-localized op-

tical and mechanical modes with resonances in the optical (1550 nm) and microwave ( $\Omega/(2\pi) \approx 5.5$  GHz) bands, respectively. The resonators are separated by a subwavelength gap,  $\text{gap}_c$ , which evanescently couples their optical modes. In contrast, their acoustic modes are uncoupled due to an efficient phononic mirror at the clamping edges of the nanobeams. A waveguide is placed laterally to one of the optomechanical cavities and used to probe the device. A photonic mirror defined in the bus waveguide ensures that the output field is efficiently collected. Finite element method simulations for the electromagnetic and acoustic modes of the system are shown in Fig. 2b. Note that  $\hat{a}_-$  ( $\hat{a}_+$ ) is associated with the symmetric (antisymmetric) optical supermode.

The devices were characterized using the setup shown in Fig. 2c, which can probe both optical and mechanical properties of the device at room temperature. The optical response is characterized by scanning the frequency of a continuous-wave tunable laser frequency (Toptica CTL 1550) while monitoring the cavity's reflection spectrum. The coupled optical modes of our system appear as two sharp resonances as Fig. 2d shows. The photon tunneling rate between the optical resonators is inferred from the mode-splitting as  $J/2\pi \approx 15$  GHz. A Lorentzian model fit to each transmission dip extracts their linewidths,  $(\kappa_-, \kappa_+)/2\pi = (546, 515)$  MHz, and extrinsic losses  $(\kappa_{e-}, \kappa_{e+})/2\pi = (153, 129)$  MHz.

The optomechanical interaction imprints information about the thermomechanical motion of the cavity onto the reflected light. Fig. 3a shows the photocurrent power spectral density,  $S_{II}(\Omega)$ , of the reflected light captured using a fast photodetector (Discovery Semiconductors DSC30S) and a real-time spectrum analyzer (Agilent PXA N9030A). Two acoustic modes were found around 5.5 GHz, corresponding to the breathing modes of each silicon nanobeam. Due to small fabrication imperfections, these modes are non-degenerate. Lorentzian fittings yields mechanical Q-factors  $Q_m \approx 2100$  for both modes. The following analysis will focus on mode 1 ( $\Omega = \Omega_1$ ), whereas analogous results for mode 2 are shown in the supplementary material (S5).

To demonstrate a unique consequence of the interference between dispersive and dissipative coupling in our device, Fig. 3b shows a density map constructed by stacking multiple photocurrent spectral densities (as in Fig. 3a) obtained for a range of laser-cavity detunings around the antisymmetric optical supermode,  $\Delta = \omega_l - \omega_+$ . The laser frequency is swept from red to blue detunings, allowing the access of  $S_{II}(\Omega)$  at  $\Delta = \pm\Omega_1$ . These are the regions of interest in the sideband-resolved regime, where either the Stokes or Anti-Stokes sidebands are resonantly enhanced. For optical powers as low as 1  $\mu$ W we verify a thermo-optically induced bistability in the optical response, causing abrupt changes in the transduction amplitude when the laser is tuned near the resonance [37, 38]. Transduction with optical power below

the bistable regime is shown in S6.

Analyzing  $S_{II}(\Omega)$  at  $\Omega = \Omega_1$  (dashed vertical line in Fig. 3b) we find a large asymmetry between the signals at  $\Delta = \pm\Omega_1$  as shown in Fig. 3c. Repeating the same experiment on the symmetric optical mode (Fig. 3d) yields a curve with the opposite features. These results cannot be explained solely within the framework of dispersive optomechanics, where symmetric curves are expected – as long as dynamical backaction is avoided, which is done by keeping a low photon occupation of  $n_c \approx 14$ . These asymmetries are compatible with a system presenting both dispersive and dissipative optomechanical couplings but have not been previously observed in the resolved sideband regime [1, 28]. For instance, in a frame rotating at the laser frequency, the phase of the stationary cavity field (dispersively scattered), is shifted by  $\approx \pi$  between red and blue detunings, whereas the waveguide field (dissipatively scattered) has a fixed phase. Consequently, the two mechanisms' interference varies from constructive to destructive between  $\Delta > 0$  and  $\Delta < 0$ . This is evident in our experiment: for the antisymmetric optical mode, we observe constructive interference between the scattering mechanisms at  $\Delta \approx \Omega_1$ , leading to enhanced transduction, in contrast to  $\Delta \approx -\Omega_1$ , where the signal is suppressed. The curves in black are theoretical estimates for  $S_{II}(\Omega)$  using a model accounting for both dispersive and dissipative couplings (see Methods) with a ratio  $G_{\kappa_{e+}}/G_{\omega_+} \approx -0.81\%$  ( $G_{\kappa_{e-}}/G_{\omega_-} \approx 1.07\%$ ) in Fig. 3c (Fig. 3d). Our results are consistent with the analysis presented in Fig. 1d, where the trends for losses  $\kappa_{\pm}$  as a function of  $\Delta\omega(x)$  are also opposite, yielding dissipative couplings with different signs.

At higher optical input powers, dynamical backaction becomes appreciable. When driving the system at frequencies resonant with Stokes ( $\Delta = \Omega_1$ ) or Anti-stokes ( $\Delta = -\Omega_1$ ) scattering processes, the amplification or cooling of the mechanical mode is observed. We anticipate an asymmetry in the efficiency of cooling and amplification processes, inherited by the same interference effects between the dispersive and dissipative scattering channels discussed above. This is in stark contrast with known results for purely dispersive optomechanical systems, where both processes are equally efficient. In the good-cavity limit,  $\Omega \gg \kappa$ , the extra damping rate of the mechanical mode,  $\Gamma^{\text{OM}}(\Delta)$ , is given by (see S3)

$$\Gamma^{\text{OM}}(\pm\Omega) \approx \mp \frac{(\mp 2\sqrt{n_c}g_\omega + g_{\kappa_e} \frac{\bar{\alpha}_{\text{in}}}{\sqrt{\kappa_e}})^2}{\kappa}, \quad (1)$$

where  $g_\omega = G_\omega x_{\text{zpf}}$  and  $g_{\kappa_e} = G_{\kappa_e} x_{\text{zpf}}$  are the dispersive and dissipative vacuum optomechanical coupling rates of (any of) the supermodes, and  $x_{\text{zpf}}$  is the zero-point fluctuation in the mechanical displacement. From Eq. 1, we expect different relative signs of  $g_{\kappa_{e\pm}}/g_{\omega_{\pm}}$  to benefit opposite backaction effects (cooling or heating). For instance, if  $g_{\kappa_-}/g_{\omega_-} < 0$  the heating process is enhanced,

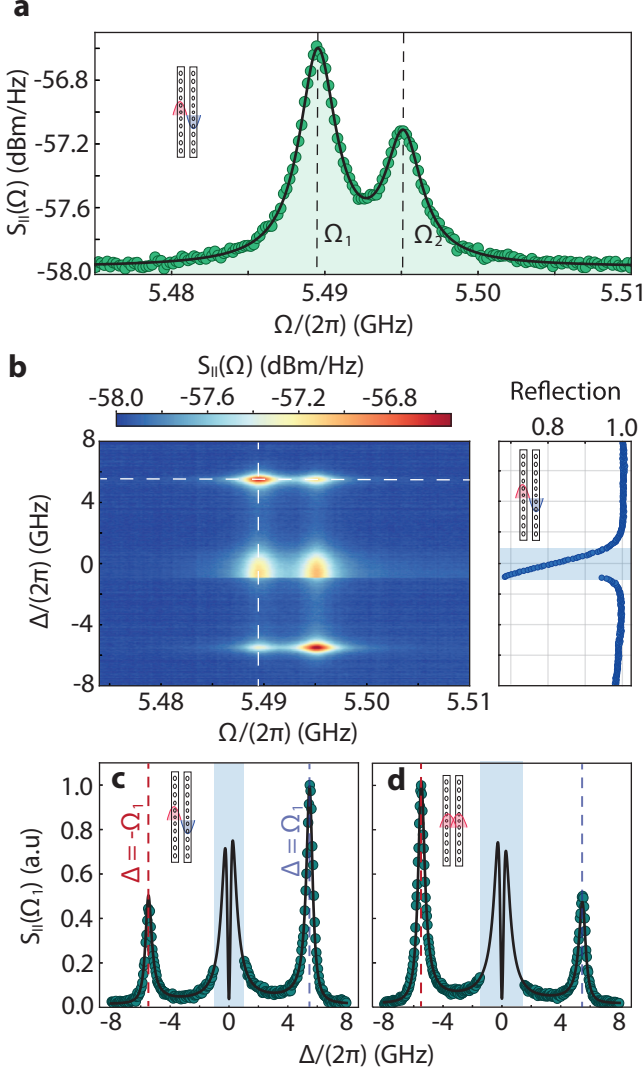


FIG. 3. **a**, Thermo-mechanical spectrum of the antisymmetric optical mode in our device at an input power  $P_{\text{in}} = 2.7 \mu\text{W}$ . Each peak corresponds to the acoustic breathing mode of individual nanobeams. **b**, Map of the mechanical spectra as a function of the laser-cavity detuning  $\Delta$ . The horizontal dashed line corresponds to **a**. The reflection spectrum at every  $\Delta$  in our measurement is also provided. **c**, Optomechanical transduction of the mechanical mode at  $\Omega_1$  for the antisymmetric optical mode. This curve corresponds to the vertical dashed line in **b**. **d**, The same analysis for the symmetric optical mode. The shaded blue region in **b** is excluded in **c** and **d**.

to detriment of cooling, whereas the converse happens if  $g_{\kappa}/g_{\omega} > 0$ . Eq. 1 also evidences the advantage of waveguide-cavity scattering: it scales with the normalized input field amplitude  $\bar{\alpha}_{\text{in}}/\sqrt{\kappa_e}$ . This is a factor  $\Omega/\kappa_e$  larger than  $\sqrt{n_c}$  in the sideband-resolved regime, enhancing the contribution from the dissipative coupling to the optomechanical interaction.

We were able to control the mechanical mode's effec-

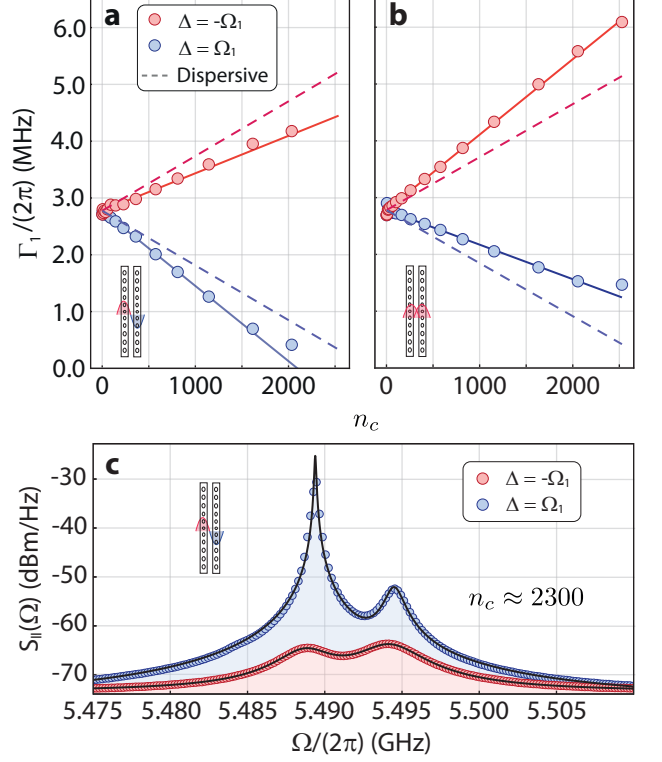


FIG. 4. Optically-induced modifications to the mechanical linewidth for the **a**) antisymmetric and **b**) symmetric optical modes, as a function of the number of photons in the resonator. Our results are compared to theoretical estimates based on a purely dispersive optomechanical resonator. **c**, Dissipative phonon lasing (blue) contrasted to optomechanical cooling (red) in the antisymmetric optical mode.

tive linewidth  $\Gamma_1$  through optomechanical cooling and heating. Results are shown in Figs. 4a and b as a function of  $n_c$ . Due to dissipative coupling, we can choose to either enhance or suppress the heating and amplification processes by pumping each supermode. For instance, the cooling efficiency relative to a purely dispersive coupling (dashed lines in Fig. 4a, b) is enhanced by roughly 40% in the symmetric mode. Such enhancement is tied to the unbalanced transduction observed under blue/red excitation observed in Figs. 3c, d. Since this is a direct consequence of the strong dissipative coupling of this system, it can be used to extract both dispersive and dissipative coupling rates. The solid lines represent fits of the full model of Eq. 1 to the experimental data, yielding  $g_{\omega+}/(2\pi) = +352(10)$  kHz and  $g_{\kappa+}/(2\pi) = -2.8(1)$  kHz ( $g_{\omega-}/(2\pi) = +356(10)$  kHz and  $g_{\kappa-}/(2\pi) = +3.8(1)$  kHz), for the symmetric (antisymmetric) optical mode. This agrees with our previous discussion where the dissipative couplings  $g_{\kappa\pm}$  were found to have similar magnitudes and opposite signals. For sufficiently large photon occupations, we achieve photon-phonon cooperativities  $C = |\Gamma^{\text{OM}}|/\Gamma > 1$  at room tem-

perature, an important metric for coherent information transfer protocols. Such large cooperativities are evidenced by Fig. 4c, where we compare the antisymmetric mode mechanical spectra under blue (red) detunings. A clear narrowing (broadening) of the mechanical mode at  $\Omega_1$  is verified. Importantly, for the blue excitation, we observe self-sustained oscillations in mechanical mode 1.

Despite the two-order of magnitude difference in the values for the different optomechanical couplings, the system's response is drastically affected when driving at  $|\Delta| = \Omega_1$ . This is a direct consequence of the waveguide-cavity scattering previously discussed: the linear dispersive optomechanical coupling scales with the number of photons in the cavity, whereas its dissipative counterpart increases with the number of photons arriving at the cavity's position through the waveguide, which is independent of  $\Delta$ . For off-resonant excitation,  $\Delta \gg \kappa$ , just a small part of the pump photons is actually converted to the cavity field, decreasing the intensity of effects arising from  $G_{\omega_{\pm}}$  in comparison to  $G_{\kappa_{e\pm}}$ . This reveals the feasibility of using waveguide-cavity scattering to increase or decrease the phononic occupation, reducing the necessity of potentially harmful pump photons,  $n_c$ , in the cavity.

Regardless of the recent progress in dissipative optomechanical systems, the observation of coherent optomechanical interactions, such as optomechanically-induced transparency or absorption (OMIT/OMIA) [26, 31, 32], remains elusive since the resolved sideband regime has not yet been reached [1, 29]. Here we overcome this barrier and demonstrate how the dissipative optomechanical interaction can either enhance or suppress such coherent effects. Our device allies large mechanical frequencies and strong dissipative couplings, making it uniquely suited for such demonstration. In OMIT, the optomechanical interaction dresses the optical response of a resonator due to photon-phonon hybridization, marking the onset of the strong-coupling regime. This is achieved by setting a carrier laser, at frequency  $\omega_l$ , such that its mechanically scattered Anti-Stokes sideband is resonant with an optical mode, i.e.,  $\Delta = -\Omega$ . The optomechanical interaction with the pump causes transitions where one phonon (population  $n_m$ ) is annihilated ( $n_m \rightarrow n_m - 1$ ) and one frequency-shifted photon (population  $n_p$ ) is created ( $n_p \rightarrow n_p + 1$ ). A probe beam, at frequency  $\omega_l + \Omega_{\text{mod}}$ , induces phonon-number conserving transitions. When  $\Omega_{\text{mod}}$  approaches  $\Omega$ , interference between mechanically scattered photons and the probe beam results in a transparency window in the probe's reflection spectrum. In our system, the depth and width of the “dip” in the optical spectrum are largely affected by both dispersive and dissipative mechanical scattering mechanisms, leading to the first observation of dissipative signatures in OMIT/OMIA. A generalized scheme for OMIT, accounting for dissipative and dispersive effects, is summarized in Fig 5a.

We assess the changes in the reflected optical spec-

tra by phase-modulating our strong input laser (carrier) and generating a weak probe beam. The modulation frequency,  $\Omega_{\text{mod}}$ , is varied using a vector network analyzer (Agilent PNA E8362C). The carrier and probe are reflected from the cavity and interfere at the fast photodiode, yielding a fluctuating photocurrent that carries the information of any optomechanical contribution to the probe's spectrum. This photocurrent is fed to the VNA which measures the scattering parameter  $S_{21}(\Omega_{\text{mod}})$  (see Methods). A typical curve for  $|S_{21}(\Omega_{\text{mod}})|$  is shown in Fig 5b, where we highlight the aforementioned transparency window, at a frequency matching the nanobeams' breathing modes.

In Fig. 5c we zoom into the transparency windows measured for both optical modes. A deeper and wider dip is observed at  $\Omega_{\text{mod}} = \Omega_1$  for the symmetric optical mode, agreeing with our previous results, where a constructive interplay of the dispersive and dissipative couplings was found when driving this same mode with a red-detuned laser. We repeat this experiment for a range of input powers and detunings  $\Delta \approx -\Omega_1$ . A model for  $|S_{21}(\Omega_{\text{mod}})|$  including optomechanical effects is fit to the data, where the ratio  $g_{\kappa_e}/g_{\omega}$  is kept fixed using the results from Fig 4. We extract the values  $g_{\omega_+}/(2\pi) = 349(8)$  kHz,  $g_{\omega_-}/(2\pi) = 373(10)$  kHz,  $g_{\kappa_{e+}}/(2\pi) = -2.8(1)$  kHz, and  $g_{\kappa_{e-}}/(2\pi) = 4.0(1)$  kHz, in excellent agreement with our previous analysis and providing evidence for the dissipative contribution to OMIT. Cooperativities extracted from OMIT are shown in Fig. 5d and compared to estimates for a purely dispersive system (dashed line). We find that  $C > 1$  is only obtained for the symmetric case when boosted by the presence of the dissipative coupling. The same conclusion could be drawn from the backaction measurements in Fig. 4b, where the dressed mechanical dissipation overcomes the intrinsic mechanical linewidth for  $n_c \approx 2500$ . Our experiments are limited by the thermo-refractive response of the cavity, which inhibits access to  $\Delta = -\Omega_1$  at large input powers. This could be overcome by cooling the present device to temperatures  $T < 20$  K, where the mechanical Q-factors are increased and optically-induced heating is reduced.

Lastly, in Fig. 5e we display complementary OMIA measurements, where the pump is set to  $\Delta \approx \Omega_1$ . This phenomenon has similar roots to the optical heating of the mechanics and therefore is more efficient (for acoustic mode 1) when driving the antisymmetric optical mode. Our theoretical model, fed with the parameters extracted from the OMIT experiments, was able to reproduce the OMIA results with great accuracy, further validating our analysis.

In conclusion, we demonstrated the first dissipative optomechanical system operating in the good-cavity regime. To the best of our knowledge, our results represent a two-order-of-magnitude leap in the acoustic frequencies (5.5 GHz) [29] with a tenfold increase in dissipa-



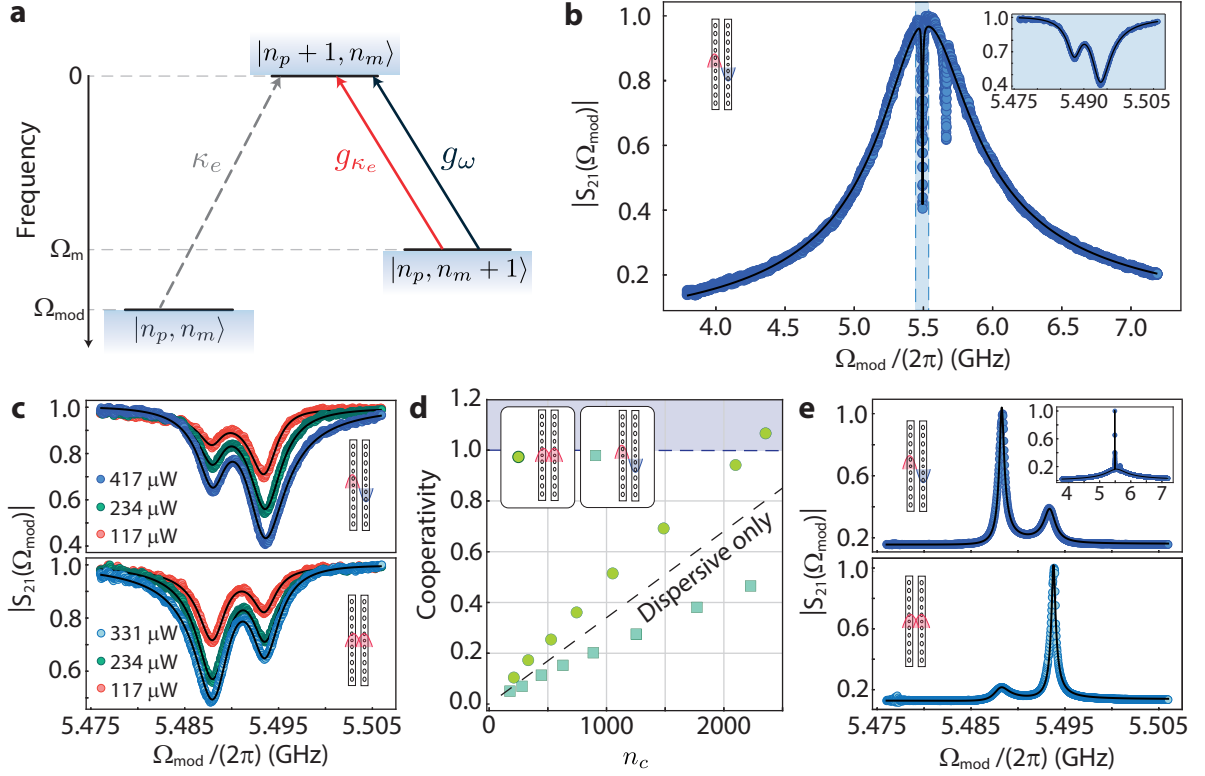


FIG. 5. **a**, Level diagram of OMIT. The probe beam induces phonon-conserving transitions while the mechanically-scattered photons necessarily decrease the phonon population. The two optomechanical coupling mechanisms (dissipative and dispersive) interfere to generate the transparency window. **b**, Scattering parameter magnitude,  $|S_{21}|$ , as a function of the phase-modulation frequency,  $\Omega_{\text{mod}}$ . Data is shown for the antisymmetric optical mode. Inset: Transparency window as highlighted in blue. **c**, Transparency windows for the antisymmetric (top) and symmetric (bottom) optical modes as a function of input power. **d**, Cooperativities for mechanical mode 1 in the symmetric and antisymmetric optical modes. Values are obtained by fitting transparency windows for several photonic occupations  $n_c$ , as exemplified in **c**. **e**, Absorption windows for the antisymmetric (top) and symmetric (bottom) optical modes. Input powers are indicated through the matching colors with **c**.

tive couplings ( $|G_{\kappa_{e\pm}}| \approx 1 \text{ GHz/nm}$ ) [28] when compared to previous literature. This allowed the first observations of strong dissipative optomechanics signatures on both optical and mechanical spectra, in spite of the small ratio between dispersive and dissipative couplings. In our system, an approximate sixfold enhancement in the dissipative coupling could be achieved solely by reducing the photon tunneling rate, enabling, for example, a nearly perfect cancellation of either the backaction heating or cooling in a given optical/mechanical mode pair. In this condition, one gains independent optomechanical control of the virtually degenerate mechanical modes 1 and 2, which is potentially interesting for quantum and classical signal processing. Further enhancement of dissipative couplings in our device is solely limited by the barrier imposed by the adiabatic regime. Complementarily, a plethora of design routes [39–41] (with integrated photonic analogs) and toolboxes [27] for dissipative optomechanics are now available in the literature and could be used to further improve our figures. As an example, increasing our measured  $g_{\kappa_e}$  for an additional order of

magnitude would put dissipative optomechanical effects on the same footing as their dispersive counterparts in state-of-the-art silicon nanobeams.

As a last remark, the waveguide-cavity scattering process discussed and demonstrated in this work remains vastly unexplored. It enables the optomechanical interaction to take place even in the absence of circulating pump photons in the cavity, which is potentially an advantage over the dispersive process. Further advances in the field could introduce devices that entirely suppress the intra-cavity field. For instance, by having a dissipative optomechanical system interact with two driving channels, set to destructively interfere at the cavity, one could effectively cloak the resonator from unwanted photons while maintaining an optomechanical interaction mediated by the waveguide photons. This could drastically reduce the noise figures in future quantum transducers and memories.

## METHODS

### Fabrication

The device manufacturing procedure follows a basic CMOS-compatible top-down approach. Electroresist polymer (CSAR-09) is spun at 2000 rpm for 1 min on top of an SOI (silicon on insulator) wafer die. The device designs are patterned on the electroresist using a 100 kV e-beam lithography tool followed by a development step immersing the chip for 1 minute in the pentyl-acetate solution. The device is then transferred to the silicon layer using a  $\text{SF}_6 + \text{O}_2$  plasma etch at cryogenic temperatures to obtain smooth walls. The residual electroresist is removed using a piranha process ( $\text{H}_2\text{SO}_4:\text{H}_2\text{O}_2 - 3:1$ ) followed by silica etch to release the structure using HF (hydrofluoric acid) solution for 3 min.

### Optomechanical Transduction

We applied input-output theory to describe the fast-detector photocurrent power spectral density  $S_{II}(\Omega)$  shown in Fig. 3. The classical optical field amplitude,  $a(t)$ , is given by

$$\dot{a}(t) = i(\Delta + G_\omega x)a(t) - \frac{\kappa + G_{\kappa_e}x}{2}a(t) - \sqrt{\kappa_e}\bar{\alpha}_{\text{in}} - \frac{G_{\kappa_e}x}{2\sqrt{\kappa_e}}\bar{\alpha}_{\text{in}}. \quad (2)$$

Linearizing this equation around stationary coherent amplitudes  $\bar{x}$  and  $\bar{a}$ , i.e.,  $a(t) \rightarrow \bar{a} + \delta a(t)$ ,  $x(t) \rightarrow \bar{x} + \delta x(t)$ , and keeping terms only to first order in the fluctuations  $\delta x(t)$ ,  $\delta a(t)$ , we arrive at the output field amplitude

$$\alpha_{\text{out}}(t) = \bar{\alpha}_{\text{in}} + \sqrt{\kappa_e}(\bar{a} + \delta a(t)) + \frac{G_{\kappa_e}\bar{a}}{2\sqrt{\kappa_e}}\delta x(t). \quad (3)$$

The photocurrent  $I(t)$  is proportional to  $|\alpha_{\text{out}}(t)|^2$ , whose fluctuations are given by  $\delta I(t) = \bar{\alpha}_{\text{out}}\delta\alpha_{\text{out}}^*(t) + \bar{\alpha}_{\text{out}}^*\delta\alpha_{\text{out}}(t)$ . Using a spectrum analyzer, one measures the power spectral density of  $\delta I(t)$ ,  $S_{II}(\omega) = \int d\tau e^{i\omega\tau} \langle \delta I(\tau)\delta I(0) \rangle$ . Finding this quantity requires moving into a frequency domain description in Eq. 3, where the optical field  $\delta a(\omega)$  is written in terms of  $\delta x(\omega)$ . Finally,  $S_{II}(\omega)$  can be written in terms of the mechanical power spectral density,  $S_{xx}(\omega)$ , which is independent of the detuning for low input powers. The transduction function between  $S_{xx}(\omega)$  and  $S_{II}(\omega)$  is given in **S2** and depends on the detuning  $\Delta$ ,  $\omega$  and other properties such as the extrinsic coupling and total losses of the optical mode under analysis.

## Optomechanically Induced Transparency

In coherent spectroscopy the input laser is phase modulated, that is,  $\bar{\alpha}_{\text{in}} \rightarrow \bar{\alpha}_{\text{in}} e^{-i\phi_0 \sin(\Omega_{\text{mod}}t)}$  in Eq. 2. For weak modulations,  $\phi_0 \ll 1$ , the system is effectively driven by a strong pump tone, at frequency  $\omega_l$  and two probes at  $\omega_l \pm \Omega_{\text{mod}}$ . In the sideband-resolved regime,  $\Omega_{\text{mod}} \gg \kappa$  and the cavity response filters out one of the probe tones. The remaining sideband induces a cavity amplitude  $a_+$ , which is given by

$$a_+ \approx - \frac{\sqrt{\kappa_e}\bar{\alpha}_{\text{in}}\phi_0}{-2i(\Delta + \Omega_{\text{mod}}) + \kappa + \frac{n_c(\Delta g_{\kappa_e} - 2\kappa_e g_\omega)^2}{\kappa_e^2(\Gamma - 2i\Omega_{\text{mod}} + 2i\Omega)}}, \quad (4)$$

where we assumed  $\Delta < 0$  and  $|\Delta| \gg \kappa$ , leading to the OMIT configuration. Here  $\Omega$  is the mechanical frequency of the acoustic mode under analysis and  $\Delta$ ,  $\kappa_e$ , and  $\kappa$  already include static shifts due to an average mechanical displacement  $\bar{x}$ .

We immediately verify that the optical susceptibility is strongly dressed by the optomechanical interaction when  $\Omega_{\text{mod}} \approx \Omega$ . This information is naturally imprinted in the reflection spectrum of the probe, which is directly connected to the magnitude of the scattering parameter  $S_{21}(\Omega_{\text{mod}})$ , measured in our experiment. A full derivation of this equation is presented in **S4**.

## ACKNOWLEDGEMENTS

This work was supported by São Paulo Research Foundation (FAPESP) through grants 19/09738-9, 20/15786-3, 19/01402-1, 18/15577-5, 18/15580-6, 18/25339-4, 22/07719-0, Coordenação de Aperfeiçoamento de Pessoal de Nível Superior - Brasil (CAPES) (Finance Code 001), the European Research Council (ERC CoG Q-ECHOS, 101001005), and by the Netherlands Organization for Scientific Research (NWO/OCW), as part of the Frontiers of Nanoscience program, as well as through Vrij Programma (680-92-18-04). We thank Prof. Fanny Béron and Prof. Kleber Pirota for providing access to the VNA used for OMIT/OMIA experiments and Dr. Felipe Santos for helpful comments.

---

\* agprimo@ifi.unicamp.br, ppinho@ifi.unicamp.br; These authors contributed equally to this work.

† alegre@unicamp.br

- [1] M. Wu, A. C. Hryciw, C. Healey, D. P. Lake, H. Jayakumar, M. R. Freeman, J. P. Davis, and P. E. Barclay, Physical Review X **4**, 021052 (2014).
- [2] T. Liu, F. Pagliano, R. van Veldhoven, V. Pogoretskiy, Y. Jiao, and A. Fiore, Nature Communications 2020 11:1 **11**, 1 (2020).



- [3] J. S. Huber, G. Rastelli, M. J. Seitner, J. Kölbl, W. Belzig, M. I. Dykman, and E. M. Weig, *Physical Review X* **10**, 021066 (2020).
- [4] C. C. Rodrigues, C. M. Kersul, A. G. Primo, M. Lipson, T. P. Alegre, and G. S. Wiederhecker, *Nature Communications* 2021 12:1 **12**, 1 (2021).
- [5] M. Zhang, G. S. Wiederhecker, S. Manipatruni, A. Barnard, P. McEuen, and M. Lipson, *Physical Review Letters* **109**, 233906 (2012).
- [6] M. Aspelmeyer, T. J. Kippenberg, and F. Marquardt, *Reviews of Modern Physics* **86**, 1391 (2014).
- [7] G. S. Wiederhecker, P. Dainese, and T. P. M. Alegre, *APL Photonics* **4**, 071101 (2019).
- [8] T. J. Kippenberg and K. J. Vahala, *Science* **321**, 1172 (2008).
- [9] X. He, G. I. Harris, C. G. Baker, A. Sawadsky, Y. L. Sfondla, Y. P. Sachkou, S. Forstner, and W. P. Bowen, *Nature Physics* 2020 16:4 **16**, 417 (2020).
- [10] W. Jiang, F. M. Mayor, S. Malik, R. Van Laer, T. P. McKenna, R. N. Patel, J. D. Witmer, and A. H. Safavi-Naeini, (2022), 10.48550/arxiv.2210.10739.
- [11] M. Mirhosseini, A. Sipahigil, M. Kalaei, and O. Painter, *Nature* 2020 588:7839 **588**, 599 (2020).
- [12] M. Forsch, R. Stockill, A. Wallucks, I. Marinković, C. Gärtner, R. A. Norte, F. van Otten, A. Fiore, K. Srinivasan, and S. Gröblacher, *Nature Physics* **16**, 69 (2020).
- [13] W. Jiang, C. J. Sarabalis, Y. D. Dahmani, R. N. Patel, F. M. Mayor, T. P. McKenna, R. Van Laer, and A. H. Safavi-Naeini, *Nature Communications* **11**, 1 (2020).
- [14] A. Rueda, F. Sedlmeir, M. C. Collodo, U. Vogl, B. Stiller, G. Schunk, D. V. Strekalov, C. Marquardt, J. M. Fink, O. Painter, G. Leuchs, and H. G. L. Schwefel, *Optica*, Vol. 3, Issue 6, pp. 597-604 **3**, 597 (2016).
- [15] S. Barzanjeh, A. Xuereb, S. Gröblacher, M. Paternostro, C. A. Regal, and E. M. Weig, *Nature Physics* 2021 18:1 **18**, 15 (2021).
- [16] A. Wallucks, I. Marinković, B. Hensen, R. Stockill, and S. Gröblacher, *Nature Physics* 2020 16:7 **16**, 772 (2020).
- [17] B. Stiller, M. Merklein, C. Wolff, K. Vu, P. Ma, S. J. Madden, and B. J. Eggleton, *Optica*, Vol. 7, Issue 5, pp. 492-497 **7**, 492 (2020).
- [18] T. P. McKenna, T. P. McKenna, J. D. Witmer, J. D. Witmer, R. N. Patel, W. Jiang, R. V. Laer, P. Arrangoiz-Arriola, E. A. Wollack, J. F. Herrmann, and A. H. Safavi-Naeini, *Optica*, Vol. 7, Issue 12, pp. 1737-1745 **7**, 1737 (2020).
- [19] X. Han, W. Fu, C.-L. Zou, L. Jiang, and H. X. Tang, *Optica*, Vol. 8, Issue 8, pp. 1050-1064 **8**, 1050 (2021).
- [20] L. Shao, M. Yu, S. Maity, N. Sinclair, L. Zheng, C. Chia, A. Shams-Ansari, C. Wang, M. Zhang, K. Lai, and M. Lončar, *Optica* **6**, 1498 (2019).
- [21] S. Hönl, Y. Popoff, D. Caimi, A. Beccari, T. J. Kippenberg, and P. Seidler, *Nature Communications* 2022 13:1 **13**, 1 (2022).
- [22] I. Shomroni, L. Qiu, D. Malz, A. Nunnenkamp, and T. J. Kippenberg, *Nature Communications* 2019 10:1 **10**, 1 (2019).
- [23] J. Chan, T. P. Alegre, A. H. Safavi-Naeini, J. T. Hill, A. Krause, S. Gröblacher, M. Aspelmeyer, and O. Painter, *Nature* **478**, 89 (2011).
- [24] N. Fiaschi, B. Hensen, A. Wallucks, R. Benevides, J. Li, T. P. Alegre, and S. Gröblacher, *Nature Photonics* 2021 15:11 **15**, 817 (2021).
- [25] F. Elste, S. M. Girvin, and A. A. Clerk, *Physical Review Letters* **102**, 207209 (2009).
- [26] T. Weiss, C. Bruder, and A. Nunnenkamp, *New Journal of Physics* **15**, 045017 (2013).
- [27] A. G. Primo, N. C. Carvalho, C. M. Kersul, N. C. Frateschi, G. S. Wiederhecker, and T. P. Alegre, *Physical Review Letters* **125**, 233601 (2020).
- [28] J. G. Huang, Y. Li, L. K. Chin, H. Cai, Y. D. Gu, M. F. Karim, J. H. Wu, T. N. Chen, Z. C. Yang, Y. L. Hao, C. W. Qiu, and A. Q. Liu, *Applied Physics Letters* **112**, 051104 (2018).
- [29] M. Li, W. H. Pernice, and H. X. Tang, *Physical Review Letters* **103**, 223901 (2009).
- [30] A. W. Barnard, M. Zhang, G. S. Wiederhecker, M. Lipson, and P. L. McEuen, *Nature* **566**, 89 (2019).
- [31] S. Weis, R. Rivière, S. Deléglise, E. Gavartin, O. Arcizet, A. Schliesser, and T. J. Kippenberg, *Science* **330**, 1520 (2010).
- [32] A. H. Safavi-Naeini, T. P. Alegre, J. Chan, M. Eichenfield, M. Winger, Q. Lin, J. T. Hill, D. E. Chang, and O. Painter, *Nature* 2011 472:7341 **472**, 69 (2011).
- [33] R. Burgwal and E. Verhagen, (2022), 10.48550/arxiv.2207.11114.
- [34] J. Xing Leong, W. Agerico Diño, A. Ahmad, a. , S. Garbe, E. Samulesson, T. J. Schmidt, T. J. Silverman, J. P. Meyers, J. J. Beaman, A. M. Jayich, J. C. Sankey, B. M. Zwickl, C. Yang, J. D. Thompson, S. M. Girvin, A. A. Clerk, F. Marquardt, and J. G. E Harris, *New Journal of Physics* **10**, 095008 (2008).
- [35] M. A. Miri and A. Alù, *Science* **363** (2019).
- [36] Y. Yanay, J. C. Sankey, and A. A. Clerk, *Physical Review A* **93**, 063809 (2016).
- [37] A. G. Primo, C. M. Kersul, R. Benevides, N. C. Carvalho, M. Ménard, N. C. Frateschi, P. L. De Assis, G. S. Wiederhecker, and T. P. Mayer Alegre, *APL Photonics* **6**, 086101 (2021).
- [38] P. E. Barclay, K. Srinivasan, and O. Painter, *Optics Express*, Vol. 13, Issue 3, pp. 801-820 **13**, 801 (2005).
- [39] A. Kato, V. Dumont, S. Bernard, J. C. Sankey, C. Reinhardt, and M. Ruf, *Optics Express*, Vol. 27, Issue 18, pp. 25731-25748 **27**, 25731 (2019).
- [40] A. K. Tagantsev and E. S. Polzik, *Physical Review A* **103**, 063503 (2021).
- [41] A. Xuereb, R. Schnabel, and K. Hammerer, *Physical Review Letters* **107**, 213604 (2011).

# Supplemental Material: Waveguide-Cavity Scattering in High-Frequency Optomechanics

André G. Primo,<sup>1,\*</sup> Pedro V. Pinho,<sup>1,\*</sup> Rodrigo Benevides,<sup>2</sup> Simon Gröblacher,<sup>3</sup> Gustavo S. Wiederhecker,<sup>1</sup> and Thiago P. Mayer Alegre<sup>1,†</sup>

<sup>1</sup>*Gleb Wataghin Institute of Physics, University of Campinas, 13083-859 Campinas, SP, Brazil*

<sup>2</sup>*Department of Physics, ETH Zürich, 8093 Zürich, Switzerland*

<sup>3</sup>*Kavli Institute of Nanoscience, Department of Quantum Nanoscience, Delft University of Technology, Lorentzweg 1, 2628CJ Delft, The Netherlands*

(Dated: January 2, 2023)

## S1. FROM AN EIGENVALUE PROBLEM TO DISSIPATIVE OPTOMECHANICS

Here we aim at deriving the existence of a dissipative optomechanical coupling using the system of coupled cavities in Fig.1b of the main text. We generalize the discussion by allowing both “bare” optical modes to display different frequencies  $\omega_1$  and  $\omega_2 = \omega_1 - \Delta\omega$ . The amplitude of the optical fields  $a_1$  and  $a_2$  are described as[1]:

$$\frac{d}{dt} \begin{bmatrix} a_1 \\ a_2 \end{bmatrix} = \begin{bmatrix} -i(\omega_1 - G_\omega x) - \frac{(\kappa_e + \kappa_i)}{2} & iJ \\ iJ & -i(\omega_1 - \Delta\omega) - \frac{\kappa_i}{2} \end{bmatrix} \cdot \begin{bmatrix} a_1 \\ a_2 \end{bmatrix} - \begin{bmatrix} \sqrt{\kappa_e} \bar{\alpha}_{\text{in}} e^{-i\omega_1 t} \\ 0 \end{bmatrix}, \quad (\text{S1})$$

which can be written in the form of  $\frac{d}{dt} \vec{a} = \mathbf{M} \cdot \vec{a} + \mathbf{J}$  and  $\bar{\alpha}_{\text{in}}$  is a coherent driving amplitude.

In the experiment, we probe this system through its supermode response, or the eigenvectors of the matrix  $\mathbf{M}$ . The eigenvalues of  $\mathbf{M}$ ,  $E_\pm$ , are given by:

$$E_\mp = -i \left( \omega_1 - \frac{\Delta\omega}{2} - \frac{G_\omega x}{2} \right) - \frac{\kappa_i}{2} - \frac{\kappa_e}{4} \pm i \sqrt{J^2 + \left[ \frac{2(-\Delta\omega + G_\omega x) + i\kappa_e}{4} \right]^2}, \quad (\text{S2})$$

which can be Taylor expanded keeping terms only to the first order in  $x$ , yielding:

$$E_\mp = -i \left( \omega_1 - \frac{\Delta\omega}{2} \right) - \frac{\kappa_i}{2} - \frac{\kappa_e}{4} \pm i \sqrt{J^2 + \left( \frac{-2\Delta\omega + i\kappa_e}{4} \right)^2} + \left( i \frac{G_\omega}{2} \mp \frac{G_\omega}{2} \frac{i2\Delta\omega + \kappa_e}{4\sqrt{J^2 + \left( \frac{2\Delta\omega - i\kappa_e}{4} \right)^2}} \right) x. \quad (\text{S3})$$

The terms independent of  $x$  define the unperturbed response of the coupled resonators. Their imaginary (real) parts correspond to the frequencies (loss rates) of the supermodes. In the notation adopted in the main text,  $E_+$  is associated with  $\omega_+$ ,  $\kappa_+$  and  $E_-$  with  $\omega_-$ ,  $\kappa_-$ . In the regime  $J \gg \kappa_e$ , corresponding to our experiment, the eigenfrequencies split into two branches. This is shown in Fig. 1c of the main text, as a function of  $\Delta\omega$ . Naturally, if  $|\Delta\omega| \gg J$  we should recover the uncoupled cavity limit. This is mathematically equivalent to taking  $J \rightarrow 0$  in the equations above. Importantly, our device operates in a regime  $\Delta\omega/J \ll 1$ , which is near optimal. In fact, for  $\Delta\omega = 0$  we note that the losses of both supermodes are identical and their frequencies differ by a factor  $2\sqrt{J^2 - \kappa_e^2/16} \approx 2J$ , indicating a perfect optical hybridization, that is,  $\omega_\pm \approx \omega_1 \pm J$  and  $\kappa_\pm = \kappa_i + \frac{\kappa_e}{2}$ . From now on, we assume  $\Delta\omega \rightarrow 0$ .

The linear terms on  $x$  generate the optomechanical coupling. For simplicity, we may consider the terms multiplying  $x$  as an effective optomechanical coupling. We have

$$\lim_{\Delta\omega \rightarrow 0} \left( i \frac{G_\omega}{2} \mp \frac{G_\omega}{2} \frac{i2\Delta\omega + \kappa_e}{4\sqrt{J^2 + \left( \frac{2\Delta\omega - i\kappa_e}{4} \right)^2}} \right) x = \left( i \frac{G_\omega}{2} \mp \frac{G_\omega}{2} \frac{\kappa_e}{4\sqrt{J^2 - \left( \frac{\kappa_e}{4} \right)^2}} \right) x, \quad (\text{S4})$$

\* agprimo@ifi.unicamp.br, ppinho@ifi.unicamp.br; These authors contributed equally to this work.

† alegre@unicamp.br

from which we see that the effective optomechanical coupling has both an imaginary and a real part, which are associated with dispersive and dissipative couplings, respectively [2]. Here, the dispersive component is divided by a factor of 2 when compared to the uncoupled cavity regime, and is identical for both supermodes, i.e.  $G_{\omega_{\pm}} = \frac{G_{\omega}}{2}$ . The effective dissipative coupling is given by

$$G_{\kappa_{e\pm}} = \mp G_{\omega} \frac{\kappa_e}{4\sqrt{J^2 - \left(\frac{\kappa_e}{4}\right)^2}}, \quad (\text{S5})$$

and associated with a modulation in the extrinsic losses, since this is the dominant loss asymmetry in our analysis. In our experiment,  $g_{\omega}/(2\pi) \approx 700$  kHz,  $\kappa_e/(2\pi) \approx 280$  MHz, and  $J/(2\pi) \approx 15$  GHz, where  $g_{\omega}$  and  $\kappa_e$  were obtained by summing the measured values of  $g_{\omega_{\pm}}$  and  $\kappa_{e\pm}$ . This is accurate since the eigenvalue treatment of the problem points out that the bare cavity dispersive coupling and extrinsic loss are, in fact, split between the two supermodes (if  $\Delta\omega \neq 0$  this splitting is uneven). Plugging the experimental values in Eq. S5, we find  $g_{\kappa_{e\pm}}/(2\pi) \approx \mp 3.26$  kHz, in excellent agreement with our measurements.

The source term in Eq. S1 is treated as follows: the eigenvectors of  $\mathbf{M}$ ,  $a_{\pm}$ , are related to  $a_1$  and  $a_2$  through:

$$\begin{bmatrix} a_+ \\ a_- \end{bmatrix} = \mathbf{P}(x) \cdot \begin{bmatrix} a_1 \\ a_2 \end{bmatrix}, \quad (\text{S6})$$

where  $\mathbf{P}(x)$  is the basis transformation matrix. If  $\Omega \ll 2J$ , i.e. the adiabatic regime, we may assume that the time variations of  $\mathbf{P}(x)$  are slow compared to those of  $a_1$  and  $a_2$ . This can be readily seen by moving into a frame rotating at the laser frequency  $\omega_l$ . In this case, we can rewrite Eq. S1 in terms of the column vector  $\vec{a}_S = [a_+, a_-]^t$  as:

$$\frac{d}{dt} \vec{a}_S = \mathbf{P} \cdot \mathbf{M} \cdot \mathbf{P}^{-1} \cdot \vec{a}_S + \mathbf{P} \cdot \mathbf{J}, \quad (\text{S7})$$

meaning the driving term is now dependent on  $x$ . The matrix  $\mathbf{P} \cdot \mathbf{M} \cdot \mathbf{P}^{-1}$  is diagonal with the eigenvalues  $E_{\pm}$  as its non-zero terms. The matrix  $\mathbf{P}$  is given by:

$$\mathbf{P}(x) = \frac{1}{\sqrt{2}} \begin{bmatrix} -1 - \frac{G_{\kappa_{e+}}}{\kappa_e} x & 1 - \frac{G_{\kappa_{e+}}}{\kappa_e} x \\ 1 + \frac{G_{\kappa_{e-}}}{\kappa_e} x & 1 - \frac{G_{\kappa_{e-}}}{\kappa_e} x \end{bmatrix}, \quad (\text{S8})$$

where we also used  $\kappa_e \ll J$  and neglected nonlinear terms in  $x$ . Finally, defining  $\kappa_{e\pm} = \frac{\kappa_e}{2}$  we have:

$$\frac{d}{dt} \begin{bmatrix} a_+ \\ a_- \end{bmatrix} = \begin{bmatrix} -i(\omega_+ - G_{\omega_+} x) - \frac{(\kappa_+ + G_{\kappa_{e+}} x)}{2} & 0 \\ 0 & -i(\omega_- - G_{\omega_-} x) - \frac{(\kappa_- + G_{\kappa_{e-}} x)}{2} \end{bmatrix} \cdot \begin{bmatrix} a_+ \\ a_- \end{bmatrix} - \begin{bmatrix} -\sqrt{\kappa_{e+}} - \frac{G_{\kappa_{e+}}}{2\sqrt{\kappa_{e+}}} x \\ \sqrt{\kappa_{e-}} + \frac{G_{\kappa_{e-}}}{2\sqrt{\kappa_{e-}}} x \end{bmatrix} \bar{\alpha}_{\text{in}} e^{-i\omega_l t}, \quad (\text{S9})$$

## S2. GENERALIZED OPTOMECHANICAL TRANSDUCTION

We turn our attention to the description of the fluctuations imprinted in the optical field due to the thermo-mechanical noise. Since our supermodes are several mechanical frequencies away from each other, we can analyze their response individually. We start from the classical optical field description:

$$\dot{a} = i(\Delta + G_{\omega} x)a - \frac{\kappa + G_{\kappa_e} x}{2} a - \sqrt{\kappa_e} \bar{\alpha}_{\text{in}} - \frac{G_{\kappa_e} x}{2\sqrt{\kappa_e}} \bar{\alpha}_{\text{in}}, \quad (\text{S10})$$

where we moved into a reference frame rotating at the laser frequency  $\omega_l$ , therefore,  $\Delta = \omega_l - \omega_c$ , where  $\omega_c$  is the mode's frequency. Here, we can associate  $a$ ,  $\Delta$ ,  $\kappa$ , and  $\kappa_e$  with either of the supermodes. We can linearize this equation around stationary coherent amplitudes  $\bar{x}$  and  $\bar{a}$  by making  $a(t) = \bar{a} + \delta a(t)$  and  $x(t) = \bar{x} + \delta x(t)$ , and keeping terms only to first order in the fluctuations. The coherent electromagnetic field is given by:

$$\bar{a} = \frac{\sqrt{\bar{\kappa}_e} \bar{\alpha}_{\text{in}}}{i\bar{\Delta} - \frac{\bar{\kappa}}{2}}, \quad (\text{S11})$$

and the dynamical part reads:

$$\dot{\delta a} = i(\bar{\Delta} \delta a + G_\omega \bar{a} \delta x) - \frac{\bar{\kappa} \delta a + G_{\kappa_e} \bar{a} \delta x}{2} - \frac{G_{\kappa_e} \delta x}{2\sqrt{\bar{\kappa}_e}} \bar{\alpha}_{\text{in}}, \quad (\text{S12})$$

where  $\bar{\Delta}$ ,  $\bar{\kappa}$ ,  $\bar{\kappa}_e$  are the renormalized detuning, total and extrinsic losses, respectively, accounting for the effects arising from a static shift in the mechanical displacement,  $\bar{x}$ .

The form of Eq. S12 allows a clear interpretation of the several sources contributing to the optical field fluctuations. First, we have the dispersively scattered part of  $\delta a$ , which is seeded by the pump photons  $\bar{a}$ . On the dissipative side, we have source terms proportional to  $\bar{a}$  and to  $\bar{\alpha}_{\text{in}}$ . The first is enhanced by the coherent part of the electromagnetic field, in the same fashion as the dispersive coupling contribution, whereas the latter is related to the waveguide-cavity scattering mechanism and is central to our discussion. In fact, for largely off-resonant excitation, which is the relevant case in sideband-resolved optomechanical systems, we have  $\bar{a} \approx \frac{\sqrt{\bar{\kappa}_e} \bar{\alpha}_{\text{in}}}{i\bar{\Delta}}$ . This is the enhancement factor for dispersive optomechanical coupling. In the case of waveguide-cavity scattering, the expression playing this same role is  $\frac{\bar{\alpha}_{\text{in}}}{2\sqrt{\bar{\kappa}_e}}$ , which is a factor  $\approx \Delta/(2\kappa_e)$  larger than its dispersive counterpart. In our experiment,  $\Delta/(2\kappa_e) \approx 20$ , justifying the large contribution from dissipative optomechanics at large detunings. Near the resonance, however, this term decreases, and so does the dissipative contribution.

The photocurrent generated at our detector is a function of the field reflected by our resonator. This is obtained through input-output relations:

$$\alpha_{\text{out}}(t) = \bar{\alpha}_{\text{in}} + \sqrt{\bar{\kappa}_e} (\bar{a} + \delta a(t)) + \frac{G_{\kappa_e} \bar{a}}{2\sqrt{\bar{\kappa}_e}} \delta x(t). \quad (\text{S13})$$

The output field  $\alpha_{\text{out}}(t)$  can also be linearized as  $\alpha_{\text{out}}(t) = \bar{\alpha}_{\text{out}} + \delta \alpha_{\text{out}}(t)$ , and fluctuating terms can be matched between the right-hand and left-hand sides of Eq. S13. The photocurrent  $I(t)$  is proportional to  $|\alpha_{\text{out}}(t)|^2$ , whose fluctuations are given by  $\delta I(t) = \bar{\alpha}_{\text{out}} \delta \alpha_{\text{out}}^*(t) + \bar{\alpha}_{\text{out}}^* \delta \alpha_{\text{out}}(t)$ . Using a spectrum analyzer, one measures the power spectral density of  $\delta I(t)$ ,  $S_{II}(\omega) = \int d\tau e^{i\omega\tau} \langle \delta I(\tau) \delta I(0) \rangle$ . Finding this quantity requires moving into a frequency domain description in Eq. S12, where the optical field  $\delta a(\omega)$  can be written solely in terms of  $\delta x(\omega)$ . We find

$$S_{II}(\omega) = \frac{16|\bar{\alpha}_{\text{in}}|^4 (-\bar{\kappa}_e + \bar{\kappa} - i\omega) (4\bar{\Delta}^2 G_{\kappa_e} - 8\bar{\Delta} \bar{\kappa}_e G_\omega + (\bar{\kappa} - 2\bar{\kappa}_e) (\bar{\kappa} - 2i\omega) G_{\kappa_e})^2}{(4\bar{\Delta}^2 + \bar{\kappa}^2)^2 (8\bar{\Delta}^2 (\bar{\kappa}^2 - 4\omega^2) + 16\bar{\Delta}^4 + (\bar{\kappa}^2 + 4\omega^2)^2)} S_{xx}(\omega), \quad (\text{S14})$$

where  $S_{xx}$  is the mechanical power spectral density. Here, we omitted a prefactor related to the particularities of the detection system used, such as signal losses, photodetector gain, and efficiency.

From Eq. S14 we can infer the transduction curves shown in Fig. 3 of the main text. There, we fix a frequency  $\omega = \Omega$ , where  $\Omega$  is the mechanical frequency, and analyze the variations of  $S_{II}(\Omega)$  as a function of  $\bar{\Delta}$ . Assuming a weak optomechanical coupling,  $S_{xx}$  is related to the bare mechanical response, in the absence of optomechanical backaction, and therefore is independent of  $\bar{\Delta}$ . As a consequence, the prefactor of  $S_{xx}$  in Eq. S14 can be used as a model for optomechanical transduction.

### S3. DYNAMICAL BACKACTION IN A DISSIPATIVE OPTOMECHANICAL SYSTEM

The Hamiltonian of a generalized optomechanical system in the presence of both dissipative and dispersive couplings is given by:  $\hat{H} = \hbar\omega_c \hat{a}^\dagger \hat{a} + \hbar\Omega \hat{b}^\dagger \hat{b} + \sum_q \hbar\omega_{q,i} \hat{c}_{q,i}^\dagger \hat{c}_{q,i} + \sum_q \hbar\omega_{q,e} \hat{c}_{q,e}^\dagger \hat{c}_{q,e} + \hat{H}_\kappa + \hat{H}_\Gamma + \hat{H}_{\text{OM}}$ . The first two terms in  $\hat{H}$  describe the bare optical and mechanical oscillators.  $\hat{H}_\kappa$  and  $\hat{H}_\Gamma$  describe the (unperturbed) damping of the optics ( $\kappa$ ) and mechanics ( $\Gamma$ ), respectively, which carry no dependency on  $\hat{x}$ . In particular, optical losses have both intrinsic and extrinsic contributions, related to the third and fourth terms describing the respective bosonic baths with subscripts “ $i$ ” and “ $e$ ”. Assuming dispersive and extrinsic dissipative optomechanical interactions, the interaction Hamiltonian  $\hat{H}_{\text{OM}}$  has the form:

$$\hat{H}_{\text{OM}} = - \left[ \hbar G_\omega \hat{a}^\dagger \hat{a} + \sqrt{\frac{\kappa_e}{2\pi\rho_e}} \frac{\hbar G_{\kappa_e}}{2\kappa_e} \sum_q (\hat{a}^\dagger \hat{c}_{q,e} - \hat{c}_{q,e}^\dagger \hat{a}) \right] \hat{x}. \quad (\text{S15})$$

Here,  $\hat{x}$  is the mechanical position operator and  $\rho_e$  denotes the density of states of the waveguide. In the Markovian limit ( $\omega_c \gg \kappa$ ), we may treat  $\rho_e$  as a constant. We assume only the coupling to the extrinsic bath modes to be affected by the mechanical displacement, ignoring the so-called intrinsic dissipative coupling. Tracing out the optical baths by means of the input-output formalism, the linearized optical force operator is  $\hat{F} = -\frac{\partial \hat{H}_{\text{OM}}}{\partial \hat{x}}$  [3, 4]

$$\begin{aligned} \hat{F}x_{\text{zpf}} &= \hbar g_\omega (\bar{a}^* \delta \hat{a} + \bar{a} \delta \hat{a}^\dagger) \\ &+ i \frac{\hbar g_{\kappa_e}}{2\kappa_e} \sqrt{\kappa_e} \left[ \bar{a}^* \delta \hat{a}_{\text{in}}^e - (\delta \hat{a}_{\text{in}}^e)^\dagger \bar{a} \right] + i \frac{\hbar g_{\kappa_e}}{2\kappa_e} \sqrt{\kappa_e} \left[ \bar{a}_{\text{in}} \delta \hat{a}^\dagger - \bar{a}_{\text{in}}^* \delta \hat{a} \right]. \end{aligned} \quad (\text{S16})$$

Here, we linearized the optical dynamics around coherent ( $\bar{a} = \langle \hat{a} \rangle$ ) and fluctuation ( $\delta \hat{a}$ ) amplitudes, in the form of  $\hat{a} = \bar{a} + \delta \hat{a}$ . The dissipation-fluctuation theorem [5] shows that the coupling to the bath modes will effectively add noise to the optical field (modeled as a fluctuating source term). In our system, this noise is intrinsic ( $\delta \hat{a}_{\text{in}}^i$ ) or extrinsic ( $\delta \hat{a}_{\text{in}}^e$ ) in nature. Since the coupling to the extrinsic bath is modulated by the mechanics,  $\delta \hat{a}_{\text{in}}^e$  also appears in the force operator.

The first line in Eq. S16 describes the force arising from the dispersive coupling, while the second is related to the extrinsic dissipative coupling. The last term is particularly interesting since it gives rise to a force directly dependent on the coherent drive amplitude through the extrinsic channel. For telecom optical photons, we may assume a zero temperature optical bath, with noise correlations:  $\langle \delta \hat{a}_{\text{in}}^J(\omega) (\delta \hat{a}_{\text{in}}^{J'}(\omega'))^\dagger \rangle = 2\pi \delta(\omega + \omega') \delta_{J,J'}$ ,  $J = e, i$ , meaning the intrinsic and extrinsic noises are uncorrelated. In the weak coupling regime, one may compute the backaction cooling/amplification of the mechanical mode from the unperturbed force's noise spectrum  $S_{\text{FF}}(\Omega)$  [3, 4, 6] and the Fermi's Golden Rule. In the present case, we have  $\delta\Gamma = \frac{x_{\text{zpf}}^2}{\hbar^2} [S_{\text{FF}}(\Omega) - S_{\text{FF}}(-\Omega)]$ . Plugging in the expression for  $S_{\text{FF}}$ , we have

$$\delta\Gamma = -\frac{4n_c\Omega}{\bar{\kappa}_e^2} \frac{\{2g_\omega g_{\kappa_e} \bar{\kappa}_e [\bar{\kappa}_e (-4\bar{\Delta}^2 + \bar{\kappa}^2 + 4\Omega^2) - 8\bar{\Delta}^2 \bar{\kappa}] + \bar{\Delta} g_{\kappa_e}^2 [4\bar{\Delta}^2 \bar{\kappa} + \bar{\kappa}_e (4\bar{\Delta}^2 - 3\bar{\kappa}^2 - 4\Omega^2) + \bar{\kappa}^3] + 16\bar{\Delta} \bar{\kappa}_e^2 \bar{\kappa} g_\omega^2\}}{16\bar{\Delta}^4 + 8\bar{\Delta}^2 (\bar{\kappa}^2 - 4\Omega^2) + (\bar{\kappa}^2 + 4\Omega^2)^2}, \quad (\text{S17})$$

where we clearly see an interplay between dispersive and extrinsic dissipative couplings. In our case,  $g_{\kappa_e} \ll g_\omega$ , and the main dissipative contributions to dynamical backaction come through crossed terms of the form  $g_\omega g_{\kappa_e}$ . Taking  $\bar{\Delta} = \pm\Omega \gg \kappa$  we recover the results in the main text.

In the main text, we use Eq. S17 to fit the values of  $\delta\Gamma$  extracted from our experiment. A taper-waveguide coupling efficiency calibration, along with the mechanical and optical spectra limit our fitting parameters to  $g_\omega$  and  $g_{\kappa_e}$ .

#### S4. OPTOMECHANICALLY INDUCED TRANSPARENCY

In this section, we derive the equations for the dressed optical susceptibility due to the optomechanically induced transparency/absorption phenomena. We start with the important remark that in coherent spectroscopy the input laser is phase modulated, that is, one needs the substitution  $\bar{\alpha}_{\text{in}} \rightarrow \bar{\alpha}_{\text{in}} e^{-i\phi_0 \sin(\Omega_{\text{mod}} t)}$  in Eq. S10. For weak modulations,  $\phi_0 \ll 1$ , we may approximate  $\bar{\alpha}_{\text{in}} e^{-i\phi_0 \sin(\Omega_{\text{mod}} t)} \approx \bar{\alpha}_{\text{in}} + \frac{\phi_0 \bar{\alpha}_{\text{in}}}{2} e^{-i\Omega_{\text{mod}} t} - \frac{\phi_0 \bar{\alpha}_{\text{in}}}{2} e^{i\Omega_{\text{mod}} t}$ , and the system is effectively driven by a strong pump tone, at frequency  $\omega_l$  and two probes at  $\omega_l \pm \Omega_{\text{mod}}$ .

The optical response to the phase-modulated input is modeled doing  $a \rightarrow \bar{a} + a_+ e^{-i\Omega_{\text{mod}} t} + a_- e^{i\Omega_{\text{mod}} t}$ . In order to simplify our discussion, we assume the pump laser is detuned several linewidths away from our optical resonance and  $\Omega_{\text{mod}} \gg \kappa$ , in accordance with experimental conditions. In this case, the optical susceptibility acts as a bandpass filter, effectively filtering one of the sidebands of our probe tones. Assuming a red-detuned laser (the OMIT configuration), the phonon-creation process is suppressed and only  $a_+$  is appreciable. Eq. S12 is rewritten as:

$$-i\Omega_{\text{mod}} a_+ = i(\bar{\Delta} a_+ + g_\omega \bar{a} b_+) - \frac{\bar{\kappa} a_+ + g_{\kappa_e} \bar{a} b_+}{2} - \frac{g_{\kappa_e} b_+}{2\sqrt{\kappa_e}} \bar{\alpha}_{\text{in}} - \sqrt{\kappa_e} \frac{\phi_0}{2} \bar{\alpha}_{\text{in}}, \quad (\text{S18})$$

where  $b_+$  is the amplitude of the phononic field oscillating at  $\Omega_{\text{mod}}$ . This quantity is obtained by solving the (classical) Langevin equation for  $b$  (obtained through the Hamiltonian of the system) with the substitution  $b \rightarrow \bar{b} + b_+ e^{-i\Omega_{\text{mod}} t} + b_- e^{i\Omega_{\text{mod}} t}$ .

The beating between the pump and probe tones will give rise to coherent mechanical oscillations, mediated by the optical force. In this classical picture, and under the same approximations above, Eq. S16 becomes

$$\begin{aligned}
Fx_{\text{zpf}} &= \hbar g_{\omega} \bar{a}^* a_+ e^{-i\Omega_{\text{mod}} t} \\
&+ i \frac{\hbar g_{\kappa_e}}{2\sqrt{\kappa_e}} \left[ \bar{a}^* e^{-i\Omega_{\text{mod}} t} \left( \frac{\phi_0}{2} e^{-i\Omega_{\text{mod}} t} - \frac{\phi_0}{2} e^{i\Omega_{\text{mod}} t} \right) - \left( \frac{\phi_0}{2} e^{-i\Omega_{\text{mod}} t} - \frac{\phi_0}{2} e^{i\Omega_{\text{mod}} t} \right)^* \bar{a} \right] - i \frac{\hbar g_{\kappa_e}}{2\sqrt{\kappa_e}} \bar{\alpha}_{\text{in}}^* a_+ e^{-i\Omega_{\text{mod}} t}.
\end{aligned} \tag{S19}$$

In our system, the second term, which is rooted in the beating between the fluctuations (or oscillations) in the input and cavity fields is necessarily smaller than the other two. This is the case since it arises from the dissipative optomechanical coupling and scales with  $\bar{a}$ . For instance, since  $g_{\kappa_e} \ll g_{\omega}$ , the dispersive term (which also scales with  $\bar{a}$ ) is obviously dominant over it. Furthermore, the last term, which is also dissipative in nature, scales with the photon flux in the waveguide, drastically increasing its importance relative to the second term. Joining all this information and writing the equation for  $b_+$ , we have

$$-i\Omega_{\text{mod}} b_+ = -\left(i\Omega + \frac{\Gamma}{2}\right) b_+ + i\hbar g_{\omega} \bar{a}^* a_+ + \frac{\hbar g_{\kappa_e}}{2\sqrt{\kappa_e}} \bar{\alpha}_{\text{in}}^* a_+, \tag{S20}$$

which can be solved for  $b_+$  in terms of  $a_+$ . Substituting this result back in Eq. S18 yields a dressed susceptibility for  $a_+$ , i.e.

$$a_+ = -\frac{\sqrt{\kappa_e} \bar{\alpha}_{\text{in}} \phi_0}{-2i(\bar{\Delta} + \Omega_{\text{mod}}) + \bar{\kappa} - \frac{n_c[(\bar{\kappa} + 2i\bar{\Delta})g_{\kappa_e} - 4i\bar{\kappa}_e g_{\omega}][(2i\bar{\Delta} + 2\bar{\kappa}_e - \bar{\kappa})g_{\kappa_e} - 4i\bar{\kappa}_e g_{\omega}]}{4\bar{\kappa}_e^2(\Gamma - 2i\Omega_{\text{mod}} + 2i\Omega)}}. \tag{S21}$$

Here, we see that the cavity response is modified by the optomechanical coupling. This is most relevant at  $\bar{\Delta} = -\Omega_{\text{mod}} = -\Omega$ . In this case, and assuming a system well into the sideband-resolved regime, we have

$$a_+ \approx -\frac{\sqrt{\kappa_e} \bar{\alpha}_{\text{in}} \phi_0}{\bar{\kappa} + \frac{n_c(2\bar{\kappa}_e g_{\omega} + \Omega g_{\kappa_e})^2}{\Gamma \bar{\kappa}_e^2}}, \tag{S22}$$

which shows an effective enhancement in the cavity losses, or, equivalently a transparency window [7, 8]. This is equivalent to what has been verified for dispersive optomechanical systems, with the addition of the dissipative contribution. We notice that, in agreement with the discussion in the main text, the transparency window is favored by  $g_{\omega}$  and  $g_{\kappa_e}$  with equal signs. This is also the case of backaction cooling under red-detuned excitation, as mentioned in the main text.

The generalization of the expressions above accounting for multiple, independent, mechanical modes (as is the case in our experiment) is done by simply adding extra optomechanical contributions to the optical response in the denominators of Eqs. S21 and S22, with modified mechanical linewidths, frequencies, and optomechanical couplings.

With this result, we are finally able to describe the scattering parameter  $|S_{21}(\Omega_{\text{mod}})|$  of the main text. This is done by using input-output relations, accounting for the phase-modulated laser. The outgoing field amplitude,  $\alpha_{\text{out}}$  reads

$$\alpha_{\text{out}} = \alpha_{\text{in}} + \sqrt{\kappa_e} a + \frac{G_{\kappa_e} a}{2\sqrt{\kappa_e}} x, \tag{S23}$$

where the last term arises from the dissipative optomechanical coupling. In the linearized regime, this term is of little relevance, since it combines the intra-cavity field  $\bar{a}$  and the dissipative coupling, which is small. Furthermore, it is not relevant for the modification of the cavity's susceptibility: it is generated by photons scattered from the cavity into the waveguide and therefore carries no information from the fluctuations in the cavity field. In that spirit, we neglect it in our analysis.

The outgoing field amplitude will have components at  $\omega_l$  and  $\omega_l \pm \Omega_{\text{mod}}$ , i.e.  $\alpha_{\text{out}} = \bar{\alpha}_{\text{out}} + \alpha_{\text{out},+} e^{-i\Omega_{\text{mod}} t} + \alpha_{\text{out},-} e^{i\Omega_{\text{mod}} t}$ . Combining this with the substitutions for the input and cavity fields, we have

$$\bar{\alpha}_{\text{out}} = \bar{\alpha}_{\text{in}} + \sqrt{\kappa_e} \bar{a} = \bar{\alpha}_{\text{in}} r(\bar{\Delta}), \tag{S24}$$

$$\alpha_{\text{out},+} = \frac{\phi_0 \bar{\alpha}_{\text{in}}}{2} + \sqrt{\kappa_e} a_+ = \frac{\phi_0 \bar{\alpha}_{\text{in}}}{2} r_{\text{OM}}(\bar{\Delta} + \Omega_{\text{mod}}), \tag{S25}$$

$$\alpha_{\text{out},-} = -\frac{\phi_0 \bar{\alpha}_{\text{in}}}{2} + \sqrt{\kappa_e} a_- = -\frac{\phi_0 \bar{\alpha}_{\text{in}}}{2} r_{\text{OM}}(\bar{\Delta} - \Omega_{\text{mod}}), \tag{S26}$$



where we defined  $r$  and  $r_{\text{OM}}$  as the “bare” and dressed cavity reflectivities, respectively. Notice that for a red-detuned laser with  $\bar{\Delta} = -\Omega$  and modulation frequency  $\Omega_{\text{mod}} = \Omega$ , the on-resonance reflectivity is probed through  $r_{\text{OM}}(\bar{\Delta} + \Omega_{\text{mod}})$ , which is directly related to  $a_+$ . This is not the case for  $r_{\text{OM}}(\bar{\Delta} - \Omega_{\text{mod}})$ , which gives the response of the cavity two mechanical frequencies away from resonance, where the optomechanical contribution to the optical susceptibility is negligible. In fact, in this case, a reasonable approximation is  $r_{\text{OM}}(-2\Omega) \approx r(-2\Omega)$ .

The scattering matrix element  $|S_{21}(\Omega_{\text{mod}})|$  is directly proportional to the output field amplitude at frequency  $\Omega_{\text{mod}}$  [9]. This is given by

$$|S_{21}(\Omega_{\text{mod}})| = \frac{\phi_0 |\bar{a}_{\text{in}}|^2}{2} |r(\bar{\Delta}) r_{\text{OM}}^*(\bar{\Delta} - \Omega_{\text{mod}}) - r^*(\bar{\Delta}) r_{\text{OM}}(\bar{\Delta} + \Omega_{\text{mod}})|, \quad (\text{S27})$$

where we omitted a scale factor. In our fittings throughout the text, an additional phase factor is introduced in order to handle any difference in the dispersion of the sidebands. This is done by making  $r_{\text{OM}}(\bar{\Delta} + \Omega_{\text{mod}}) \rightarrow r_{\text{OM}}(\bar{\Delta} + \Omega_{\text{mod}}) e^{i\psi}$ . Our fitting parameters are chosen to be  $\bar{\Delta}$ ,  $\psi$ , and  $g_\omega$ , with all the other parameters extracted from independent measurements shown in Figs. 2-4 in the main text.

## S5. ANALYSIS FOR ACOUSTIC MODE 2

The results in Section S1 can be readily extended to the more realistic scenario in which each optical resonator is coupled to its own acoustic mode. Consider the system of coupled cavities in Fig. 1b of the main text, where each optical resonator displays different resonance frequencies  $\omega_i$ ,  $i = 1, 2$ , and coupled to independent acoustic modes with mechanical displacement  $x_i$  through a dispersive coupling  $G_{\omega_i}$ . The generalization of the matrix  $\mathbf{M}$  for this particular system is given by

$$\mathbf{M} = \begin{bmatrix} -i(\omega_1 - G_{\omega_1} x_1) - \frac{(\kappa_e + \kappa_i)}{2} & iJ \\ iJ & -i(\omega_2 - G_{\omega_2} x_2) - \frac{\kappa_i}{2} \end{bmatrix}. \quad (\text{S28})$$

Once more, we are interested in the case where the frequencies of the bare optical resonators are degenerate, i.e.  $\omega_2 = \omega_1$ . Taylor expanding  $\kappa_\mp$  and  $\omega_\mp$  up to first order in the  $x_i$ , we obtain:

$$\begin{aligned} \kappa_\pm &= \kappa_i + \kappa_e \left( \frac{1}{2} \mp \frac{G_{\omega_1}}{4\sqrt{J^2 - (\kappa_e/4)^2}} x_1 \pm \frac{G_{\omega_2}}{4\sqrt{J^2 - (\kappa_e/4)^2}} x_2 \right), \\ \omega_\pm &= \omega_1 \pm 4\sqrt{J^2 - (\kappa_e/4)^2} - \frac{1}{2} (G_{\omega_1} x_1 + G_{\omega_2} x_2). \end{aligned} \quad (\text{S29})$$

One can then define a dissipative (dispersive) coupling  $G_{\kappa_{e\pm}}^{(i)}$  ( $G_{\omega_\pm}^{(i)}$ ) associated to acoustic mode  $i$ :

$$G_{\kappa_{e\pm}}^{(i)} = \frac{d\kappa_\pm}{dx_i} = \begin{cases} \mp \frac{G_{\omega_i} \kappa_e}{4\sqrt{J^2 - (\kappa_e/4)^2}}, & i = 1, \\ \pm \frac{G_{\omega_i} \kappa_e}{4\sqrt{J^2 - (\kappa_e/4)^2}}, & i = 2, \end{cases} \quad (\text{S30})$$

$$G_{\omega_\pm}^{(i)} = -\frac{d\omega_\pm}{dx_i} = \frac{G_{\omega_i}}{2}. \quad (\text{S31})$$

In addition to recovering Eq. S5 in the  $G_{\omega_2} \rightarrow 0$  limit, Eq. S31 also reveals that  $G_{\kappa_{e\pm}}^{(1)} = -G_{\kappa_{e\pm}}^{(2)}$ , meaning the sign of the dissipative coupling is flipped between different acoustic modes. This asymmetry between the behaviors of mechanical modes 1 and 2 is generated due to the fact that only one of the optical cavities is coupled to the waveguide. Furthermore, the dispersive coupling maintains its sign irrespective of the mechanical modes,  $G_{\omega_\pm}^{(1)} = G_{\omega_\pm}^{(2)}$ , implicating that optomechanical interactions dependent on the interplay between dispersive and dissipative coupling will display opposing behaviors between the different mechanical modes.

In our experiment, acoustic modes 1 and 2 correspond to the independent mechanical breathing modes of the nanobeams. A frequency mismatch between them, due to fabrication imperfections, enables their individual analysis of the impacts of the mechanically mediated waveguide-cavity interaction.

From the thermo-mechanical spectrum map presented in the main text, it is also possible to analyze  $S_{II}(\Omega)$  at  $\Omega = \Omega_2$  as a function of the detuning  $\bar{\Delta}$ . An asymmetry in the signal of  $S_{II}(\Omega_2)$  between  $\bar{\Delta} = \pm\Omega_2$  is observed in Fig. S1a), rooted in the same interference process between dissipative and dispersive coupling discussed in the main text. The nature of this interference is constructive (destructive) for  $\bar{\Delta} = -\Omega_2$  ( $\bar{\Delta} = \Omega_2$ ) when the antisymmetric

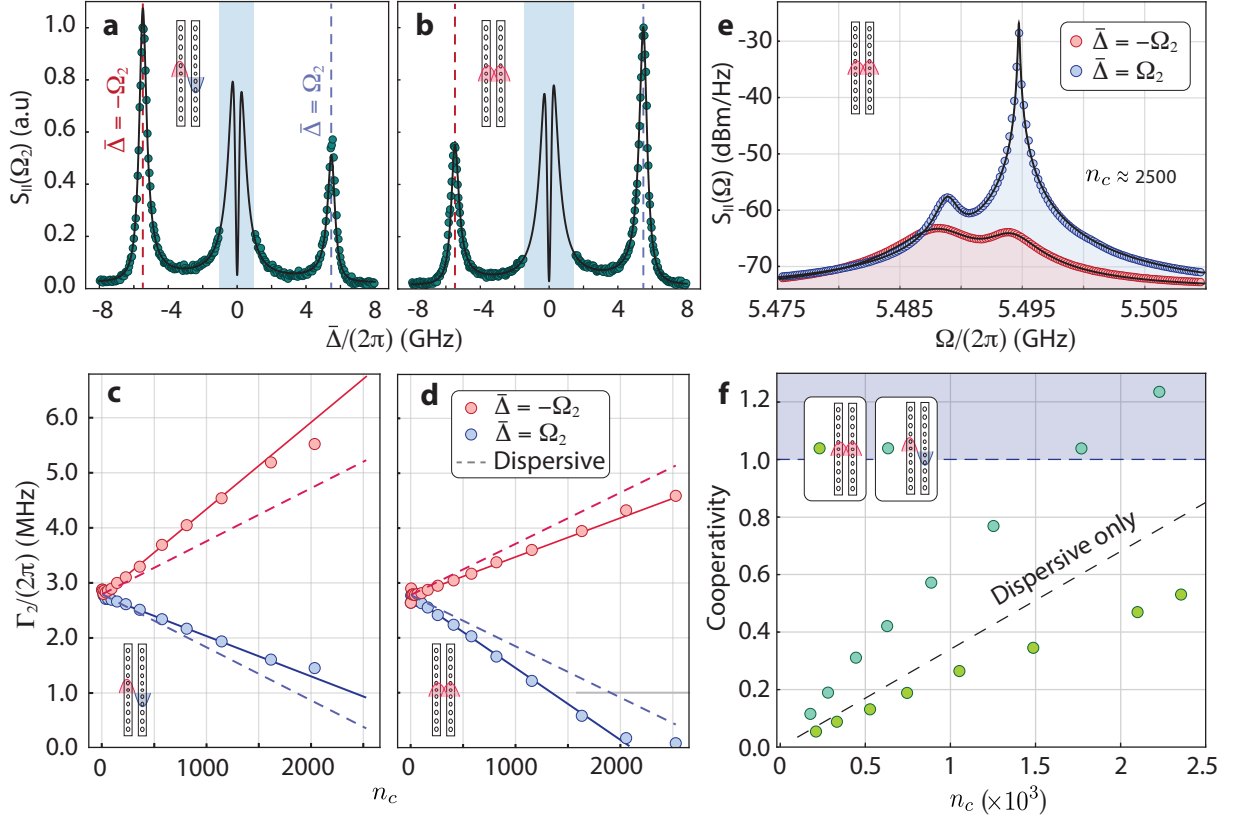


FIG. S1. Optomechanical transduction of the acoustic mode at  $\Omega = \Omega_2$  for the antisymmetric (a) and symmetry (b) optical mode with the shaded region in blue around the optical resonance excluded. Optically-induced modifications to the mechanical linewidth of the acoustic mode at  $\Omega = \Omega_2$  for the antisymmetric (c) and symmetric optical modes (d), as a function of the number of photons in the resonator, the dashed lines represent the case of a purely dispersive system. (e) Dissipative phonon lasing (blue) contrasted to optomechanical cooling (red) in the symmetric optical mode. (f) Cooperativities for mechanical mode 2 in the symmetric and antisymmetric optical modes.

optical mode is analyzed. The converse behavior is observed for the symmetric mode, as seen in Fig. S1b), owing to its opposite sign for  $G_{\kappa_e}$ . The asymmetries in the transduction spectra of mechanical mode 2 are exactly opposite to those of mechanical mode 1, shown in the main text. For instance, while the anti-Stokes (Stokes) process is enhanced in Fig. S1a (b), it is suppressed in Fig. 3 c (d) of the main text. This is a direct consequence of the results obtained for  $\Omega = \Omega_1$  and will persist for the remaining analysis. In the same spirit of the main text, the curves in black are theoretical estimates for  $S_{II}(\Omega)$  using the model derived in Eq. S14 with  $G_{\kappa_e+}^{(2)}/G_{\omega+}^{(2)} \approx 0.0089$  for the antisymmetric optical mode and  $G_{\kappa_e-}^{(2)}/G_{\omega-}^{(2)} \approx -0.0085$  for the symmetric mode.

Optomechanical damping was also analyzed for  $\Omega = \Omega_2$ . Results are shown in Fig. S1c and d where the asymmetry between the Stokes ( $\bar{\Delta} = \Omega_2$ ) and anti-Stokes ( $\bar{\Delta} = -\Omega_2$ ) scattering processes efficiency was also observed. For the antisymmetric mode, we find optomechanical cooling to be enhanced and heating suppressed when compared to the purely dispersive case, as observed in Fig. S1c. The solid lines represent a fit using the model derived in Eq. S17, yielding  $g_{\omega+}^{(2)}/(2\pi) = 378.5(8)$  kHz and  $g_{\kappa_e+}^{(2)}/(2\pi) = 3.37(6)$  kHz. The flip in the relative sign between dispersive and dissipative couplings for the symmetric mode translates into a suppression of the cooling mechanism and enhancement of the heating, as observed in Fig. S1d). For this case, fitting of the experimental data yields  $g_{\omega-}^{(2)}/(2\pi) = 367(1)$  kHz and  $g_{\kappa_e-}^{(2)}/(2\pi) = -3.11(9)$  kHz. We note that for the highest optical power used for the symmetric mode, mechanical mode 2 is driven to self-sustained oscillations under blue-detuned optical excitations, as shown in Fig. S1e). We stress that this would not be observed for a purely dispersive system under the same experimental conditions.

By coherently driving the system at resonance with the Anti-Stokes sideband,  $\bar{\Delta} = -\Omega_2$ , OMIT measurements for both optical modes were performed as a function of the photonic occupation,  $n_c$ . Cooperativities of the system were measured by fitting the transparency window through the model for  $|S_{21}(\Omega_{\text{mod}})|$  derived in Eq. S27. The results are shown in Fig. S1f) and compared to the case of a purely dispersive system (dashed line). Cooperativities greater than

unity were achieved at lower input powers when probing the antisymmetric optical mode. Such results are expected given that, for this optical mode, the dispersive and dissipative coupling interfere constructively with  $\Delta = -\Omega_2$ , as seen in the results of dynamical backaction and optomechanical transduction.

## S6. NEARLY COLD-CAVITY TRANSDUCTION

In the main text we displayed transduction curves (described by Eq. S14) in the absence of backaction. This was done to keep  $S_{xx}(\Omega)$  constant as a function of detuning. Experimentally, this is achieved by keeping sufficiently low input powers. However, due to the high Q-factors and small modal volumes of our silicon devices, powers as low as 1  $\mu$ W trigger nonlinear optical effects such as thermo-optical dispersion, two-photon absorption, and (consequently) free-carrier absorption and dispersion [10, 11]. This is manifested in the optical spectra of our device, which is shown to be bistable in Fig. 3b of the main text.

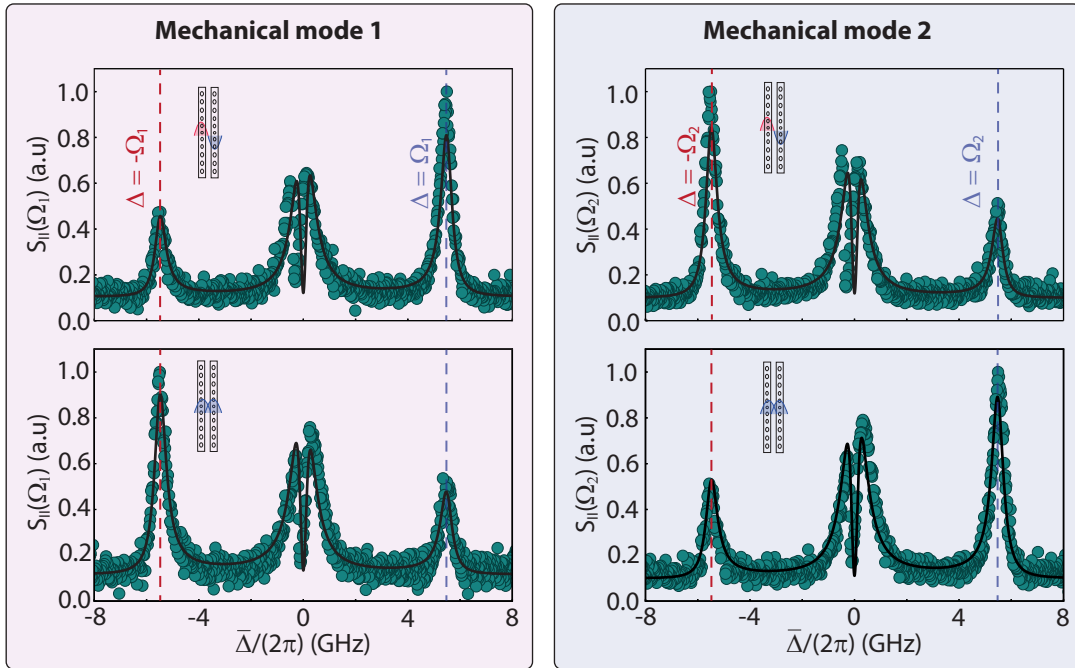


FIG. S2. Optomechanical transduction for mechanical modes 1 (left) and 2 (right), under excitation of the antisymmetric (top) and symmetric (bottom) optical modes.

In Fig. S2 we show the transduction spectra of mechanical modes 1 and 2 outside the optical bistable regime. We readily verify that the same asymmetries between red and blue-detunings is maintained for all combinations of optical and acoustic modes, in accordance with previously shown results. Furthermore, the black curves are the same theoretical estimates used before which were based on the values of dissipative and dispersive couplings extracted from backaction/OMIT experiments. The agreement between theory and experiment is poorer than for higher-power data. We attribute this to the low signal-to-noise ratio of the mechanical spectra for low optical powers and to a slight thermo-refractive shift of the resonance under near-resonant excitation.

*Note.* – Data, FEM and script files for generating each figure will be available at the *Zenodo* repository.

- 
- [S1] H. Haus, *Waves and Fields in Optoelectronics* (Prentice-Hall, 1984).
  - [S2] Y. Yanay, J. C. Sankey, and A. A. Clerk, *Physical Review A* **93**, 063809 (2016).
  - [S3] F. Elste, S. M. Girvin, and A. A. Clerk, *Physical Review Letters* **102**, 207209 (2009).
  - [S4] T. Weiss, C. Bruder, and A. Nunnenkamp, *New Journal of Physics* **15**, 045017 (2013).
  - [S5] R. Kubo, *Reports on Progress in Physics* **29**, 255 (1966).
  - [S6] A. G. Primo, N. C. Carvalho, C. M. Kersul, N. C. Frateschi, G. S. Wiederhecker, and T. P. Alegre, *Physical Review Letters* **125**, 233601 (2020).

- [S7] A. H. Safavi-Naeini, T. P. Alegre, J. Chan, M. Eichenfield, M. Winger, Q. Lin, J. T. Hill, D. E. Chang, and O. Painter, *Nature* 2011 472:7341 **472**, 69 (2011).
- [S8] S. Weis, R. Rivière, S. Deléglise, E. Gavartin, O. Arcizet, A. Schliesser, and T. J. Kippenberg, *Science* **330**, 1520 (2010).
- [S9] I. Shomroni, L. Qiu, D. Malz, A. Nunnenkamp, and T. J. Kippenberg, *Nature Communications* 2019 10:1 **10**, 1 (2019).
- [S10] A. G. Primo, C. M. Kersul, R. Benevides, N. C. Carvalho, M. Ménard, N. C. Frateschi, P. L. De Assis, G. S. Wiederhecker, and T. P. Mayer Alegre, *APL Photonics* **6**, 086101 (2021).
- [S11] P. E. Barclay, K. Srinivasan, and O. Painter, *Optics Express*, Vol. 13, Issue 3, pp. 801-820 **13**, 801 (2005).